California High-Speed Rail Authority

Palmdale to Burbank Project Section

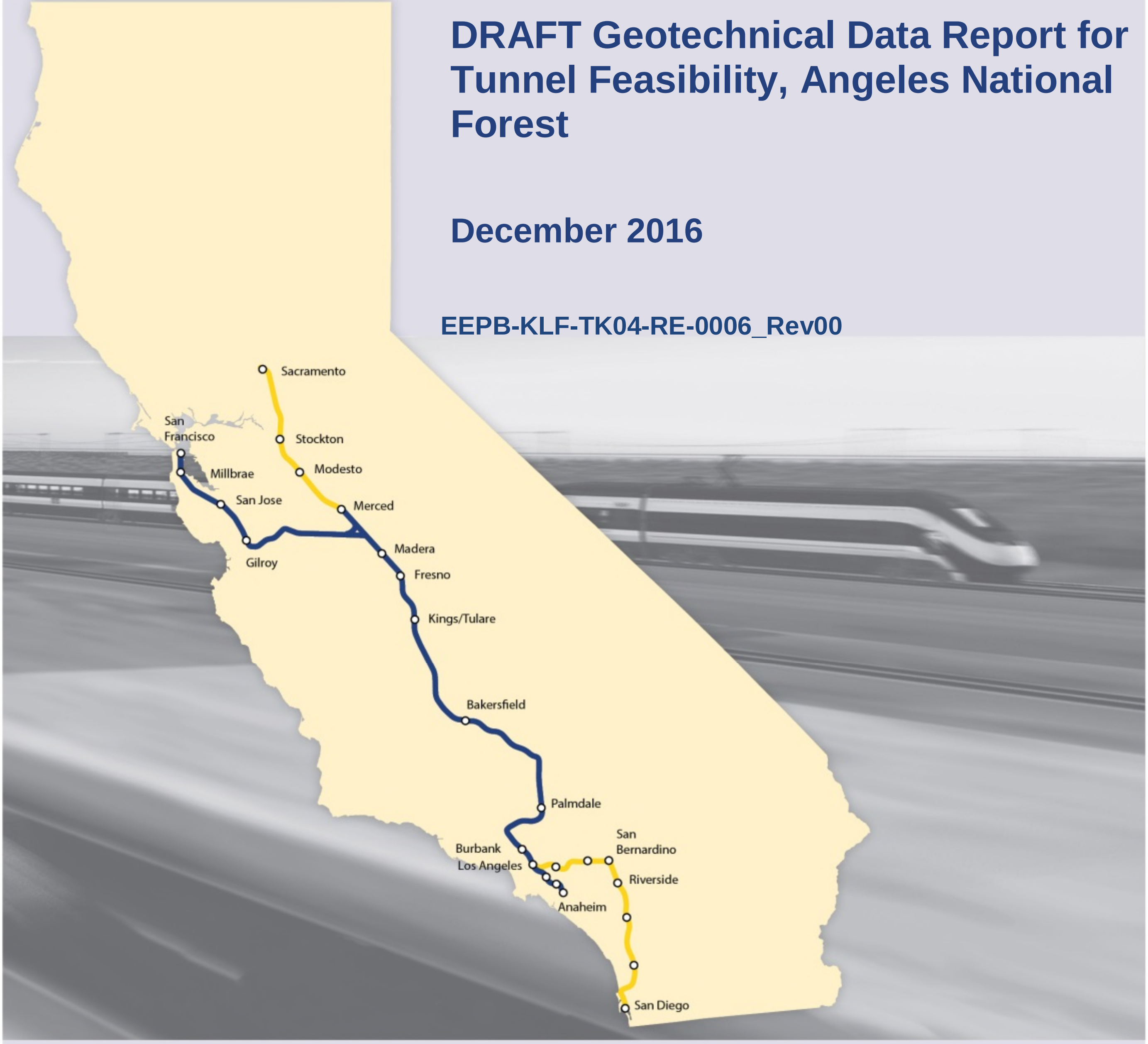

DRAFT Geotechnical Data Report for Tunnel Feasibility, Angeles National Forest

December 2016

EEPB-KLF-TK04-RE-0006_Rev00

CALIFORNIA
High-Speed Rail Authority

U.S. Department
of Transportation
Federal Railroad
Administration

	Name	Signature	Date
Prepared by	Adam Williams, PE Geotechnical Engineer, Kleinfelder		
Checked by	Name, Title and Company		
Approved by	Name, Title and Company		

Signature not needed if electronically approved by route

DOCUMENT EVOLUTION LOG		
Revision	**Description**	**Date**
00	Initial Edition. Issued for Approval	12/21/16

TABLE OF CONTENTS

Tables

Figures

Appendices

ACRONYMS AND ABBREVIATIONS

A	activity
Authority	California High-Speed Rail Authority
ANF	Angeles National Forest
ASTM	ASTM International
bgs	below ground surface
$Ca\text{-}HCO_3$	calcium bicarbonate
$Ca\text{-}SO_4$	calcium sulfate
$Ca\text{-}HCO_3/Ca\text{-}SO_4$	calcium sulfate/calcium chloride
CAI	Cerchar Abrasiveness Index
CAL	caliper
Caltrans	California Department of Transportation
CDMG	California Division of Mines and Geology
CGS	California Geological Survey
CH	Fat CLAY
CHSR	California High-Speed Rail
CL	Lean CLAY
cm/sec	centimeters per second
CSU	California State University
d-excess	deuterium excess
DIC	dissolved inorganic carbon
DO	dissolved oxygen
DOGGR	California Division of Oil, Gas, and Geothermal Resources
DPH	Department of Public Health
DWR	California Department of Water Resources
EC	electrical conductivity
EIR	Environmental Impact Report
EIS	Environmental Impact Statement
EMI	Earth Mechanics Institute
$F^{14}C$	fraction modern carbon
FHWA	Federal Highway Administration
FRA	Federal Railroad Administration
FTC	fluid temperature and conductivity
GAMA	Groundwater Ambient Monitoring and Assessment
GDRTF	Geotechnical Data Report for Tunnel Feasibility

GI Plan	Geotechnical Investigation Plan
GMWL	global meteoric water line
GSI	Geological Strength Index
HFZ	hazardous fault zone
HiRAT	high-resolution acoustic televiewer
HRC	Rockwell Hardness Scale
HSR	High-Speed Rail
IAEA	International Atomic Energy Agency
IRMS	Isotope Ratio Mass Spectrometry
ISRM	International Society for Rock Mechanics
JRC	joint roughness coefficient
km	kilometer
LACDPH	County of Los Angeles Department of Public Health
LACDPW	County of Los Angeles Department of Public Works
LADWP	Los Angeles Department of Water and Power
LI	liquidity index
meq/L	milliequivelants per liter
mg/L	milligram per liter
m_i	Hoek-Brown material constant
Mm	moment magnitude
Mmax	maximum moment magnitude
MPa	megaPascal
mS/cm	milliSiemens per centimeter
MSL	mean sea level
mV	millivolt
$Na\text{-}HCO_3$	sodium bicarbonate
NCDC	National Climate Data Center
NHD	National Hydrography Dataset
NHFZ	non-hazardous fault zone
NIST, formerly NBS	US National Institute of Science and Technology
NOAA	National Oceanic and Atmospheric Administration
NP	non-plastic
NPS	National Park Service
NTU	Nephelometric Turbidity Units
ORP	Oxidation Reduction Potential
pCi/L	picocurie per liter

pH	potential of hydrogen
Phase 1	first phase
PHFZ	potentially Hazardous Fault Zone
pMC	percent modern carbon
PMT	Program Management Team
psi	pounds per square inch
psi/ft	pounds per square inch per foot
pcf	pound per cubic foot
Q	Rock Mass Quality
QA/QC	Quality Assurance and Quality Control
QC	Quality Control
QHSE	Quality, Health, Safety and Environment
QMP	Quality Management Plan
RC	regional consultant
RMR	Rock Mass Rating
RQD	Rock Quality Designation
SC	Clayey SAND
SCAMP	Southern California Aerial Mapping Project
SGFZ	San Gabriel Fault Zone
SM	Silty SAND
SMOW	Standard Mean Ocean Water
SP	spontaneous potential
SP-SM	Poorly-graded SAND with Silt
SPR	single point resistance
SR	State Route
SR-14	State Route 14
SUP	Special Use Permit
SUSP	Oyo P-S wave suspension
SWRCB	California State Water Resources Control Board
SW-SM	Well-graded SAND with Silt
TBM	tunnel boring machine
TDS	total dissolved solids
TU	tritium units
µg/L	microgram per liter
UCERF3	Uniform California Earthquake Rupture Forecast, Version 3
USBR	US Department of the Interior, Bureau of Reclamation
USCS	Unified Soils Classification System

USDA	United States Department of Agriculture
USFS	United States Forest Service
USGS	United States Geological Survey
years BP	years before present
VPDB	Vienna Pee Dee Belemnite
VWP	vibrating wire piezometer
VWPT	vibrating wire pressure transducer
XRD	x-ray diffraction

EXECUTIVE SUMMARY

The California High-Speed Rail (HSR) Authority (Authority) proposes to construct, operate, and maintain an electric-powered HSR system in California. When completed, it will run from San Francisco to the Los Angeles Basin in under 3 hours at speeds capable of exceeding 200 miles per hour. The system will eventually extend to Sacramento and San Diego, totaling 800 miles with up to 24 stations.

The Authority and the Federal Railroad Administration (FRA) have prepared program-wide, Tier 1 environmental documents for the HSR system under the California Environmental Quality Act (CEQA) and the National Environmental Policy Act (NEPA). Specifically, the Authority and FRA prepared the Statewide Program Environmental Impact Report/Environmental Impact Statement (EIR/EIS) (Authority and FRA 2005) to evaluate the ability of the HSR system to meet the existing and future capacity demands on California's intercity transportation system. The Authority and FRA also prepared the Bay Area to Central Valley HSR Program EIR/EIS (Authority and FRA 2008) to identify a corridor alignment and the station locations for the connection between the Bay Area and the Central Valley.

The Authority and FRA are now undertaking second-tier, project environmental evaluations for several sections of the statewide system. This report is for the Palmdale to Burbank Project Section. This project section is approximately 38- to 44-mile long, and has multiple alignment alternatives under study. The project section extends through a variety of land uses and ecoregions, including urban, rural, and mountainous terrain. Each alignment alternative would involve areas of tunneling beneath the Angeles National Forest (ANF), including portions within the San Gabriel Mountains National Monument (SGMNM).

Each of the alternatives under analysis in the Palmdale to Burbank Project Section is divided into three subsections: Palmdale, Central and Burbank.

This report presents the data from a limited geotechnical investigations (GI) for the feasibility of tunnels beneath the Angeles National Forest and San Gabriel Mountains National Monument within the Central Subsection of the Palmdale to Burbank Section. The fieldwork was conducted by the authority of the Organic Administration Act of June 4, 1897 under Special Use Permit LAR823A issued by the US Department of Agriculture Forest Service to the California High Speed Rail Authority.

The GI consisted of the following: review of available relevant information; limited surface geologic mapping; drilling and coring five borings within the ANF to core depths ranging from 1,004.7 to 2,702.7 feet; geophysical surveys and in-situ testing; laboratory testing; and installation of instruments within the core holes.

1 INTRODUCTION

The planning, design, construction, and operation of the California High-Speed Rail (HSR) System are the responsibility of the California High-Speed Rail Authority (Authority), a state governing board formed in 1996. The Authority’s statutory mandate is to develop an HSR system coordinated with the state’s existing transportation network, including intercity rail and bus lines, regional commuter rail lines, urban rail and bus transit lines, highways, and airports. The Authority’s plans call for high-speed intercity train service on more than 800 miles of track throughout California, connecting the major population centers of Sacramento, the San Francisco Bay Area, the Central Valley, Los Angeles, the Inland Empire, Orange County, and San Diego. Implementation of the California HSR System is planned in two phases. Phase 1 would connect San Francisco to Los Angeles and Anaheim through the Central Valley. Phase 2 would connect the Central Valley (Merced Station) to Sacramento, and another extension is planned from Los Angeles to San Diego. The HSR system would meet the requirements of Proposition 1A, including maximum, nonstop service travel time between San Francisco and Los Angeles of two hours and 40 minutes.

The Palmdale to Burbank Project Section would be a critical link in the Phase 1 HSR system connecting San Francisco and the Bay Area to Los Angeles and Anaheim. In 2005, the Authority and the Federal Railroad Administration (FRA) relied on Program Environmental Impact Report/Environmental Impact Statement (EIR/EIS) documents to select the SR-58/Soledad Canyon and LACMTA/Metrolink corridors as the preferred alignment between Bakersfield and Sylmar, with a station in the City of Palmdale. This alignment would extend east from Bakersfield along SR-58, generally following SR-58 through the Tehachapi Mountains to Mojave, along LACMTA/Metrolink corridors through Antelope Valley and Soledad Canyon, and generally follow SR-14 from the City of Santa Clarita to Sylmar in the City of Los Angeles. (FRA 2005). The SR-58/Soledad Canyon and LACMTA/Metrolink corridor from Bakersfield to Los Angeles was later split into two sections for more detailed project-level evaluation: the Bakersfield to Palmdale Section and the Palmdale to Los Angeles Section.

The alternatives for the Palmdale to Los Angeles Section were then defined through public scoping conducted for the Palmdale to Los Angeles Section in 2007, the alignment and station screening evaluation process described in the Palmdale to Los Angeles Preliminary Alternatives Analysis Report (PAA) (2010), and the Palmdale to Los Angeles Supplemental Alternatives Analysis (SAA) Reports (2011, 2012, and 2014).

A recommendation in the 2014 SAA Report in May 2014 was that the Palmdale to Los Angeles Section be divided into two sections (Palmdale to Burbank and Burbank to Los Angeles). Following this recommendation, a second public scoping period took place from July to September 2014. Following this public scoping period, the Palmdale to Burbank SAA Report (2015) was presented to the Authority Board of Directors in June 2015.

Subsequently, during the June 9, 2015 Board meeting, issues were raised regarding the alternatives presented in the 2015 SAA. Subsequent to the Board meeting, the Authority explored ways to refine the alternatives to address concerns raised at the Board meeting and through previous stakeholder outreach. The 2016 SAA, presented to the Authority Board of Directors in April of that year, reflects refinements to the rail alignments, stations, and ancillary features presented in the 2015 SAA.

The Palmdale to Burbank Project Section would be a critical link in the California HSR System, connecting the San Francisco Bay Area to Los Angeles and Anaheim and is the subject of this technical report. For evaluating the feasibility of tunnels beneath the Angeles National Forest, the Authority developed and implemented a geotechnical investigation plan (GI Plan) within the ANF to collect data pertinent to the tunnel feasibility. Three alternative alignments are currently being considered through the ANF, the SR-14 alignment traversing the mountains west of Bear Divide and two eastern alignments, E1 and E2.

The subject of this technical report is the geotechnical feasibility of deep mountain tunnels beneath the Angeles National Forest (ANF) and part of San Gabriel Mountains National

Monument for the Palmdale to Burbank Project Section. Three alignment options are under environmental study for this section, which would be approximately 38 to 44 miles long from station to station. The Palmdale to Burbank Project Section would extend through a variety of geological terrain and widely varying geotechnical and groundwater conditions. This report summarizes geotechnical conditions only within the ANF. Future studies will include additional geotechnical investigations within and outside of the ANF, as needed.

This report documents the technical description of the geotechnical data obtained within the ANF for the Central Subsection, Palmdale to Burbank Section of the California HSR System.

This report includes the following:

- Description of background geotechnical and geological data within the ANF both published and collected during this geotechnical investigation;
- Description of field, laboratory and analytical methods for data compilation of rock quality, and in-situ conditions; and
- Documentation of rock core logs, results of field and laboratory tests, drilling progress, core photography, and instrumentation readings.

1.1 Project Description

The approximately 38- to 44-mile Palmdale to Burbank Section has multiple alignment alternatives under study. The project section extends through a variety of land uses and ecoregions, including urban, rural, and mountainous terrain. Each alignment alternative would involve areas of tunneling beneath the Angeles National Forest (ANF), including portions within the San Gabriel Mountains National Monument (SGMNM).

1.2 Alternatives

This section briefly describes the Palmdale to Burbank Project Section alternatives (SR-14, E1, and E2), including the No Project Alternative. Please refer to the Supplemental Alternatives Analysis (Authority 2016) for a discussion of alternatives that were considered but eliminated from further consideration in the EIR/EIS.

1.2.1 No Project Alternative

The No Project Alternative assumes that the Palmdale to Burbank Section would not be constructed.

In assessing future conditions, it was assumed that all currently known, programmed, and funded improvements to the intercity transportation system (highway, rail, and transit) and reasonably foreseeable local development projects (with funding sources already identified) would be developed as planned by 2040. With regard to other HSR sections, the No Project future condition assumes that only those project sections with Tier 2 environmental clearance as of September 2016 would be constructed or operational, which includes the Merced to Fresno and Fresno to Bakersfield project sections. No other Southern California project sections are assumed to be constructed or operational under the No Project future condition.

The No Project Alternative is based on a review of all city and county general plans, regional transportation plans for all modes of travel, and agency-provided lists of pending and approved projects within Los Angeles County.

1.2.2 High-Speed Rail Build Alternatives

The HSR Build Alternatives for the Palmdale to Burbank Project Section include three (SR-14/E1/E2) end-to-end alternatives. In Appendix A, A.1 and A.2 with Exploratory Core Hole Locations show the alignment alternatives and station options. Discussion of the HSR Build Alternatives is organized from north to south.

Within the ANF of the Central Subsection, the SR-14 alignment is separate from the other two alignments but joins E2 south of the ANF boundary. The E1 and E2 alignments share a common course beneath the San Gabriel Mountains National Monument and then diverge southward into separate alignments through the ANF.

1.2.3 E1 Alternative

The northern limit of the E1 alternative enters the San Gabriel Mountains National Monument near Station 638+00. It traverses by tunnel beneath the National Monument for approximately 3 miles emerging in Aliso Canyon from Station 725+19 to 747+85, 0.42 miles, where it enters the National Monument again in tunnel. From Station 750+00 to 860+00, E1 continues in tunnel beneath Arrastre Canyon, exiting briefly the ANF between Station 860+00 and Station 916+00. The alignment enters the north edge of the National Monument at Station 916+00 and continues in tunnel to the south side of the Angeles National Forest near Station 1620+00 a distance of 13.3 miles. Near Station 1110+00, the E1 alternative leaves the National Monument and transitions to the Angeles National Forest (ANF). The maximum depth of the tunnel invert is south of forest road 3N17 Santa Clara Divide at 2,100 feet below ground.

1.2.4 E2 Alternative

The E2 and E1 alternatives follow the same path in the San Gabriel National Monument from Station 680+00 until Station 1020+00, where E2 takes a more easterly alignment passing beneath North Fork Station and continuing below Pacoima Canyon and then passing beneath Mendenhall Ridge. It continues south to the edge of the ANF at Station 1625+00. The maximum depth to the tunnel is at Mendenhall Ridge, where the tunnel invert is 2,650 feet below the ground surface.

1.2.5 SR-14 Alternative

The northern limit of the SR-14 Central Subsection is near Lang Station at the northern edge of the San Gabriel Mountains National Monument, Station 1320+00, where a portal is located on the Vulcan Mine property south of the Santa Clara River crossing. The alignment trends southwest and exits the National Monument briefly near Station 1470+00. It enters the ANF at Sand Canyon near Station 1530+00 and crosses beneath the mountains west of Bear Divide. The tunnel leaves the ANF at Station 1705+00 but continues underground where it joins the E1 alignment south of the ANF boundary. The length of the tunnel starting at the Vulcan Mine portal to the southern edge of the ANF is approximately 7.3 miles. The highest topographic relief is within the ANF where maximum cover over the tunnel invert is 2,100 feet.

1.3 Purpose

The primary purpose of the geotechnical investigations in the ANF was to evaluate subsurface conditions that could have a strong bearing on the feasibility of tunnel design and construction within the ANF. The Study Area encompasses approximately 25 square miles of the higher elevations (3,000 to 4,500 feet mean sea level [MSL]) within the ANF containing the three tunnel alignments, extending from west of Bear Divide eastward to North Fork Station and southward to the San Gabriel fault. Exploration sites were selected to investigate in-situ rock conditions, the ground conditions at fault crossings, and to measure groundwater pressures and hydraulic conductivities along the deepest tunnel locations beneath the mountains. Key parameters affecting tunnel feasibility include water pressures, hydraulic conductivities, potential water flow, ground conditions at significant fault zones, and ground temperatures. The test borings were planned and implemented for the purpose of obtaining in situ field measurements of these key parameters in the areas of highest ground cover, where maximum limits of pressure, potential groundwater flow and temperature can be measured. The test borings provide data to help evaluate potentially challenging conditions for construction within the ANF by investigating in-situ rock stresses, adverse geology, including faults and gouge zones, and squeezing ground.

1.4 Scope of Work

The Authority outlined a desired scope of work for the planned field investigations that detailed the field activities, exploration locations and access, purpose, exploration methods and precautions to protect the forest environment. Since the geotechnical investigations were conducted within the Angeles National Forest, the US Forest Service (USFS) had authority over the mitigation requirements to be met while working in the field. The scope of services was submitted to the USFS for review and comment. The USFS provided their comments prior to the Authority finalizing the work scope in a geotechnical investigation plan (GI Plan, CHSRA, 2015a). The GI Plan addressed the USFS concerns and included mitigation measures for environmental protection and mitigation.

The GI Plan outlined proposed test locations and an overall approach for the geotechnical investigation for the alternatives being considered by the Authority within the ANF. The GI Plan was prepared in general accordance with relevant CA HSR Technical Memoranda.

The implementation of the GI Plan was authorized under a Special Use Permit (SUP) issued by the USFS. The SUP included summaries of the proposed field investigations, descriptions of each of the drill sites, and the results of environmental surveys for biological and archaeological resources.

A total of five (5) HQ wireline rock cores holes were drilled within the ANF. Three borings (E1-B2, FS-B1, and ALT-B2) were angled borings, drilled at approximately 65 degrees plunge from horizontal to intersect faults and pass through faults below the groundwater table. Two deep vertical core holes (E1-B1 and ALT-B3) were drilled to depths below the anticipated elevation of the tunnel alignments. The rock cores were logged, photographed and boxed at each drill site.

The following tasks were completed for the GI program:

- Continuous rock coring at five sites (FS-B1, E1-B1, E1-B2, ALT-B2, and ALT-B3) to depths of 1,004.7; 2,702.7; 1,005.9; 1,617.8; and 2,100.2 feet below ground surface (bgs), respectively;
- Geologic Logging of 8,431.3 feet of cored rock;
- Outdoor-lighted high resolution photography of each core run prior to placement in core boxes;
- Transportation of rock core boxes to a temporary storage and processing facility;
- In-situ hydraulic conductivity testing using single or dual packer systems;
- In situ groundwater sampling;
- In-situ rock stress/strength testing;
- Geophysical logging including caliper, electric (spontaneous potential), temperature, conductivity, natural gamma, seismic velocity, and downhole televiewer surveys; and
- Installation of vibrating wire pressure transducers (VWPTs) within each hole.

At the completion of drilling and testing, each 4-inch diameter core hole was abandoned in accordance with County of Los Angeles and State of California regulatory guidelines for well drilling and abandonment.

The following activities were conducted at the core storage facility:

- Receive and inventory rock core boxes;
- Detailed check of field rock core log for Quality Control (QC);
- High-resolution photography of rock core both wet and dry under controlled lighting;
- Core sample selections for laboratory testing of mechanical properties; and
- Core sample selections for petrographic analyses.

After completion of rock coring and installation of vibrating wire pressure transducers (VWPT) in each core hole, dataloggers were installed and programmed, and in-situ measurements were downloaded. The scope of work included the following activities:

- Installation of battery operated dataloggers and connection to wire leads of each VWPT;
- Take periodic readings and download of data from loggers; and
- Data reduction and graphic plots of temperature and water pressure.

1.5 Project Datum

The locations of the core holes were surveyed for horizontal and vertical controls referenced in geodetic coordinates for latitude and longitude and California Coordinate System used by Caltrans. Elevations were referenced in feet above sea level for vertical coordinate locations.

The following were used for the project datum:

- Horizontal Control
  - Geodetic Coordinate Datum;
  - NAD 83 (NSRS 2007);
  - Epoch 2007 (PB-CHSR Control);
  - California Coordinate System 5; and
  - NAD 83, US Survey Feet
- Vertical Control
  - North American Vertical Datum 88; and
  - Orthorhombic Datum in Feet

1.6 Report Organization

This report is divided into two major parts: 1-the main text with tables and references to figures, and references; 2- the Appendices, where results of data analyses and testing are compiled.

The first part of this report contains six sections as follows: Section 1 is the Introduction containing project information, the basis of planning field investigations, scope, and the quality management plan. Background information is in Section 2, which describes climate, physiography, geology and tectonics and hydrogeology. Section 3 details the field activities conducted for the field investigation including geologic mapping, the rock coring exploration methods and in situ geophysical surveys and testing program. Section 4 presents the laboratory testing for rock and soil, petrography, groundwater chemistry and environmental testing. The results of the field investigations are presented in Section 5 of this report, which contains summaries of data collected from vibrating wire piezometer transducer (VWPT) readings, geophysical surveys, groundwater chemistry, in-situ testing, laboratory testing, and rock mass characterization. Section 6 contains the references used in support of the data collection, compilation, and analyses.

The second part of this report (Appendices) contains the detailed data collected during this ANF GI Plan implementation. The appendices are divided into ten sections as follows:

Appendix A – Maps and Profiles; Appendix B – Report Figures; Appendix C – Drilling Summaries; Appendix D – Rock Core Borings; Appendix E – Petrography; Appendix F – Instrumentation; Appendix G – Geophysical Surveys; Appendix H – In-Situ Testing; Appendix I – Soil and Rock Laboratory Testing; Appendix J – Groundwater Laboratory Testing; Appendix K – Rock Mass Characterization

1.7 Quality Management Program

The quality management program implemented for the geotechnical field investigations data collection, data analysis, and data presentation was based on the Quality Management Plan (QMP) developed for the project dated August 2015, Rev 2 (CAHSR 2015b). The QMP guides the project activities regarding Quality Control and Quality Assurance (QA/QC) processes and the roles and responsibilities of the project team regarding the mentioned activities.

2 BACKGROUND INFORMATION

2.1 Other Studies

The geological and hydrogeological information provided in this report is, in part, based on a review of the research conducted by various investigators mentioned below and cited in Section 6. In using this information, the Project Team has assumed it reasonably represents the conditions at the exploration locations investigated. We have performed limited field reconnaissance, geologic mapping, subsurface exploration, and laboratory testing to support and/or supplement the geologic information from previous studies of the western San Gabriel Mountains and Study Area.

Numerous maps and reports were reviewed as part of this study, including published maps and reports from academic researchers, and from local, state and federal government sources. State sources of information include; the California Geological Survey (CGS) formerly the California Division of Mines and Geology (CDMG), California Division of Oil, Gas, and Geothermal Resources (DOGGR), Los Angeles Department of Water and Power (LADWP), Los Angeles Department of Public Works (LADPW), California Department of Water Resources (DWR). The federal agencies included the U.S. Geological Survey (USGS), United States Forest Service (USFS), United States Department of Agriculture (USDA), and the National Oceanic and Atmospheric Administration (NOAA).

The CGS (Campbell, et.al., 2014; Saul and Wootton, 1983; Oakeshott, 1958), Dibblee (1991a, 1991b and 1996a-c), USGS (Yerkes and Campbell, 2005), and Carter (1980a) provided general surface mapping of the Study Area’s geology. Additionally, surficial landslide mapping and seismic hazard maps and reports by the CGS Seismic Hazard Zonation Program, USGS topographic maps (for the Sunland, San Fernando, Mint Canyon, Condor Peak, Acton and Aqua Dulce 7.5-minute quadrangles), as well as, aerial photographs (USDA) were reviewed for existing surface geohazards, such as, landslides and/or faulting.

Reports and maps specific to the bedrock formations, lithology and geologic conditions underlying the Study Area and the western San Gabriel Mountains were reviewed. These include Carter (1980a), Oakeshott (1958), Ehlig (1975a and b), Silver (1971) and Campbell and others (2014). Subsurface geologic information provided in historical boreholes and well data from DOGGR and LADPW were utilized. Assessment for faulting, rupture hazard and ground shaking hazard were provided by several sources including the USGS and CGS fault database (2006). Other specific fault hazard sources include: Weber, 1982 (San Gabriel fault), Nourse, 2002 (San Gabriel fault), Cotton, 1986 (San Gabriel fault), Murphy, 1973 (San Fernando earthquake and related faults), Lindvall and Rubin, 2003 (San Fernando earthquake), Barrows and others, 1974 (San Fernando earthquake and related faults), and Crook and others, 1987 (Sierra Madre fault zone).

Hydrogeolgical data of groundwater resources from the USGS and the California State Water Resources Control Board (Davis and Shelton, 2014), USGS Hydrography Dataset website, and available water well data from LADPW were utilized.

2.2 Climate

The climate of the Los Angeles region of southern California varies between subtropical on the Pacific Ocean side of the San Gabriel Mountain range to arid in the Mojave Desert. The climate of the mountain range is Mediterranean, with mostly dry summers (except for rare summer thunderstorms) and cold, wet winters (Bailey 1966). Snow can fall above 4,000 feet elevation during frontal passages of winter storms between November and April, but is most common in December through March. The snowfall generally melts rapidly except on higher peaks and the northern slopes. Snow is rarely experienced on the San Fernando Valley (LACDPW, 2015). Nearly all precipitation occurs during the months of December through March. Precipitation during summer months is infrequent, and rainless periods of several months are common. Annual precipitation totals are mostly above 25 inches above 3,000 feet elevation, with up to 40 inches falling in some areas above 5,000 feet and can be extremely high during wet "El Nino" years, sometimes over 70 inches, with single storm totals over 10 inches. The coastal side (San

Fernando Valley) of the San Gabriel Mountain range receives more precipitation than the Mojave Desert, but generally less than the mountains. Runoff from the mountains during big storms often produces flooding in adjacent foothill communities (especially in areas denuded by wildfires).

In mountain areas, the steep canyon slopes and channel gradients promote a rapid concentration of storm runoff. Soil moisture during a storm has a pronounced effect on runoff from the porous soils supporting deep-rooted vegetation such as chaparral. Soil moisture deficiency is greatest at the beginning of a rainy season, having been depleted by the evapotranspiration process during the dry summer months. Precipitation during periods of low soil moisture is nearly completely absorbed by soils, and except for periods of extremely intense rainfall, significant runoff does not occur until soils are wetted to capacity. Due to high infiltration rates and porosity of mountain soils, runoff occurs primarily as subsurface flow or interflow in addition to direct runoff. Spring or base flow is essentially limited to portions of the San Gabriel Mountain range. Consequently, most streams in the mountains are intermittent (LACDPW, 2015).

At times, the climate can be influenced by offshore winds from the east. Between September and March, a high-pressure system over the Great Basin, combined with a low-pressure system to the southwest, creates warm, dry winds that circulate through the region. Known as the Santa Ana winds, these winds have a significant impact on the local climate of the San Gabriel Mountains. After the long dry summers, the Santa Ana winds contribute to the fire regime, which begins in the summer season and continues until the wet winter ensues.

The San Gabriel Mountain range blocks the moist sea air, creating an arid, desert climate north of the San Gabriel Mountains in the Mojave Desert. Also, the San Gabriel Mountain range and hills surrounding the San Fernando Valley can prevent horizontal air movements in the valley creating temperature inversions that promote conditions where smog stays in the environment. Although the valley is impacted, the San Gabriel Mountain range is mostly smog free above 5,000 feet elevation, above the inversion layer (National Park Service [NPS], 2013).

2.3 Physiography

The Project is located within Angeles National Forest (ANF) in the western part of the San Gabriel Mountains. The San Gabriel Mountains are located within the central part of the 300-mile long, east-west trending Transverse Ranges Geomorphic Province (California Geological Survey [CGS], 2002). The Transverse Ranges are characterized by a complex series of mountain ranges, intervening valleys, and active faults with dominant east-west trends. The east-west trend of the Transverse Ranges, which are an exception to California's predominantly northwest structural grain, are the consequence of active faulting and folding that is driven by movement along San Andreas fault Zone, the boundary between the North American and the Pacific crustal plates.

In the Project area, the San Fernando Valley and the San Gabriel Mountains are the principal constituents of the Transverse Ranges geomorphic province. The San Fernando Valley is an east-west-trending structural trough that has subsided and filled with sediment as the adjacent San Gabriel Mountains have risen. The San Gabriel Mountains are composed of an igneous-metamorphic complex that is overlain along the southern and northern margins by folded and faulted sedimentary rocks of Pliocene and Pleistocene age. The San Gabriel Mountains owe their present height to mid-Pleistocene-to-recent uplift along generally east-west-trending, northerly dipping reverse faults that border the southern front of the range (Ehlig 1975a). The mountains are considered one of the fastest growing mountain ranges in the world, rising as much as 0.75 inches (2 centimeters) per year (LADPW, 2014). Because the San Gabriel Mountains have experienced considerable uplift in recent geologic time, the range has become a rugged mountain block that is deeply dissected with steep-walled canyons with slopes are as steep as 65 to 70 degrees. The canyons provide surface water drainage to the north into Soledad Canyon/Santa Clara River, and to the south into the San Fernando Valley, generally via Big Tujunga or Little Tujunga Canyons.

North of San Fernando Valley, the San Gabriel Mountains crest abruptly from the south at Santa Clara Divide, a drainage divide ranging in elevation from approximately 2,700 feet to over 6,500 feet. Pacoima, Little Tujunga, and Big Tujunga Canyons cut through the range south of Santa Clara Divide, carrying runoff into the Tujunga Wash and San Fernando Valley. Little Tujunga Canyon Road bridges the range in this area, connecting the San Fernando Valley to the Santa Clara River valley in the north through Bear Divide. Towering over Big Tujunga Canyon north of Big Tujunga Reservoir is Mount Gleason, which at 6,502 feet is the highest peak in this region of Study Area. Other notable peaks in the Project vicinity include Magic Mountain (elevation 4,890 feet), Mendenhall Peak (elevation 4,660 feet) and Kagel Mountain (elevation 3,537 feet). Magic Mountain is located along the Santa Clara Divide, which crosses the SR-14 alignment at about Station 1620+00. Mendenhall Peak is located along Mendenhall Ridge, another drainage divide that crosses the E2 alignment at about Station 1335+00. Kagel Mountain overlooks Pacoima Reservoir to the north and is located along a southerly extension of Mendenhall Ridge, crossing the E1 alignment at about Station 1600+00.

North of the Santa Clara Divide, the topography descends incrementally northward and more gradually than the mountain's southern flanks. The northern boundary of the Study Area coincides with the northern boundary of the ANF, which roughly follows the upper Santa Clara River and Soledad Canyon. In this area, the Santa Clara River and the Soledad Canyon are at an elevation of approximately 1,600 to 2,800 feet. Within the Study Area, the E1 and E2 alignments remain south of, and do not cross, the Santa Clara River or the Soledad Canyon. However, the SR-14 alignment crosses Soledad Canyon at approximately Station 1305+00 near the Lang Southern Pacific Railroad Station. Runoff from these northern slopes of the San Gabriel Mountains drain north into Soledad Canyon. Intermittent flow in Soledad Canyon is to the west where it enters the Santa Clara River near the SR 14 alignment crossing of the canyon. From these headwaters, the Santa Clara River will flow westward until emptying into the ocean in Ventura.

2.4 Regional Geologic Setting

The San Gabriel Mountains are a prominent geologic structural feature of the Transverse Ranges geomorphic province that have experienced a complex tectonic history. In the Study Area, the San Gabriel Mountains are bounded by the San Andreas Fault Zone to the north and San Fernando Valley to the south. The rocks exposed in the core of the mountains are of metamorphic and intrusive igneous origin and range in age from Proterozoic to Miocene. The margin of the mountains are mantled with Tertiary-age sedimentary rocks (siltstone and sandstone), particularly near Soledad Canyon and Santa Clara River Valley, to the north and west, and along the southern flanks of the mountain above San Fernando Valley (Figure A.3). Since early Miocene, the mountains along with the rest of the Transverse Ranges experienced clockwise rotation due to the transitional plate boundary movements along the right-lateral San Andreas Fault (Atwater, 1998). Movement of the present-day alignment of the San Andreas fault including the compressional "big bend" feature is speculated to have occurred over the past 5 million years (Atwater 1998) and facilitated the northeast movement of the San Gabriel Mountains from the present-day Salton Trough (Nourse, 2002; and USGS, 2004).

The San Gabriel Mountains form a basement massif that includes components of Proterozoic to late-Cretaceous metamorphic and plutonic rocks. These are the oldest basement rocks in the Los Angeles area and appear to represent old continental crust at the western margin of the North American craton that have been thrust over Jurassic oceanic crust. The San Gabriel Mountains consists of two geologic terranes, the Mesozoic Pelona Schist (lower plate) and a complex of Proterozoic to Cretaceous metamorphic and igneous rocks (upper plate), separated by the (inactive) Vincent thrust fault. The metamorphic rocks are primarily Proterozoic (1.7 to 1.2 billion years old) gneisses, which have been intruded by a plutonic anorthosite-gabbro complex, which is also Proterozoic in age. The Proterozoic rocks have been subjected to additional episodes of Mesozoic intrusions including the Triassic-age (220 million years old) Mount Lowe Granodiorite intrusive suite and younger granitic and volcanic intrusions about 105 to 80 million years ago (Silver, 1971; Ehlig, 1975b). Over the next approximate 60 million years, the San Gabriel Mountains would lie low on the horizon, as marine layers of sedimentary rock are deposited along its margin. This included the Eocene- to Miocene-age Juncal, Sespe, Vasquez, Tick, Mint Canyon, Modelo, and Towsley Formations. Uplift of the San Gabriel Mountains began about 16 million years ago (Beyer et.al. 2009; McCulloh, Beyer and Morin, 2001) exposing the sedimentary layers on the flanks of the San Gabriel Mountains. However, the San Gabriel Mountains proper began to acquire their modern configuration during the early Pleistocene but did not reach their present height until late Pleistocene and Holocene time. Streams emanating from the mountains deposited the non-marine Saugus Formation along the southern flanks of the mountains adjacent to the ancient San Fernando basin. The sedimentary rock layers extend into the subsurface of the current San Fernando Valley and subsequently have been covered by alluvial deposits.

The San Andreas Fault System formed along the translational boundary between the North American and Pacific Plates in Miocene. Convergent transform movements are responsible for the mountain building of the Transverse Ranges and the San Gabriel Mountains. The east-west oriented Transverse Ranges/San Gabriel Mountains present an anomaly in southern California where all the other mountain ranges are oriented parallel to the strike of the San Andreas Fault System. Paleomagnetic data indicate that the Transverse Ranges was originally oriented north-south, with its southern and northern ends located near the latitude of present day San Diego and Anaheim, respectively (Atwater, 1998; Kamerling and Luyendyk, 1985). During the evolution of the Pacific-North America plate boundary, the Transverse Ranges broke off the North America plate and rotated as a cohesive block 80-110 degrees clockwise to its present position (Kamerling and Luyendyk, 1985). This process of rotation, which was associated with faulting, folding, and crustal upwelling in the Transverse Ranges, continued until about 5 million years ago. The development of the San Gabriel fault, generally regarded as an older strand of the San Andreas Fault System occurred during this time (Atwater, 1998). In addition to the San Gabriel fault, other active faults belonging to the San Andreas Fault System which have formed in the Project area the past few million years include the Sierra Madre (Sunland and San Fernando strands), and Verdugo faults (Figure A.4). The San Gabriel Mountains owe their steep, youthful southern front to the uplift to the reverse faults belonging to the Sierra Madre fault. However, there are many faults within the San Gabriel Mountains, which affect the development of the geologic structure, stratigraphy and hydrogeology of the Project area, but are not considered active (i.e., experienced displacement in the past 11,000 years), although sympathetic movement could occur. These include, Agua Dulce, Pole Canyon, Oak Spring, Magic Mountain, Lonetree, Transmission Line, Laurel Canyon, Goose Berry Canyon, Bad Canyon, Mendenhall, and Slaughter Canyon faults (Figure A.5). These inactive faults promote canyon development and erosion by juxtapose differing lithologies/formations and promote and/or restrict groundwater movement within the interconnected fracture networks.

The geology of the San Gabriel Mountains is very complex because of multiple stages of metamorphism, igneous intrusion, rotation, and faulting. However, more recently the uplift of the mountains has followed a relatively simple pattern of reverse faulting along the southern margin and broad arching along the northern margin (Ehlig, 1975a). A simple pattern that continues today. The San Fernando earthquake of 1971 provides proof that range uplift is still going on and that earthquakes are likely to occur along other faults of the range front within the foreseeable future.

2.5 Tectonics and Seismicity

The Study Area, like most of California, is tectonically active and has produced large historical earthquakes associated with the San Andreas Fault Zone (Wallace, 1990; Powell et al., 1993), and the oblique left-lateral reverse tectonic faults in the Transverse Ranges (Crook et al., 1987). The San Andreas Fault Zone has produced numerous earthquakes including the 1857 magnitude (M) 7.8 Fort Tejon earthquake (Sieh, 1978). In 1971, the Sylmar earthquake (M 6.6) occurred on the Sierra Madre (San Fernando strand) (U.S. Geological Survey Staff, 1971). Other significant historic earthquakes that have occurred near the Study Area include:

- The 1769 Los Angeles Basin earthquake (M 6.0) on an undetermined fault;
- The 1812 Wrightwood earthquake (M 7.3) on the San Andreas Fault;
- The 1827 Santa Monica Bay earthquake (M 6.0) on an undetermined fault;
- The 1855 Los Angeles Basin earthquake (M 6.0) on an undetermined fault;
- The 1857 Fort Tejon earthquake (M 7.8) on San Andreas Fault;

- The 1933 Long Beach earthquake (M 6.4) on the Newport-Inglewood fault;
- The 1971 Sylmar earthquake (M 6.6) on the Sierra Madre fault;
- The 1987 Whittier Narrows earthquake (M 6.0) on the Puente Hills Thrust Fault; and
- The 1994 Northridge earthquake (M 6.7) on the Northridge Thrust Fault.

The project Study Area will be subjected to future seismic shaking during earthquakes generated by any of several surrounding active faults. The locations of the known active and potentially active faults in the Study Area are shown on the Local Geologic Map, provided as Figure A.5. However, the area could be subjected to ground shaking caused by regional faults outside the Study Area. The intensity of the ground motion at the Study Area depends upon the distance to the fault rupture, the earthquake magnitude, and the geologic conditions underlying and surrounding the Study Area. Table 2-1, "Summary of Potential Seismic Sources with 100 Kilometers of the Project Study Area" provides a listing of the potential seismic sources, and fault characteristics, within 100 kilometers of the Study Area.

Table 2-1 Summary of Potential Seismic Sources within 100 Kilometers of the Project Site

Fault Name	Fault Length miles (km)	Fault Type with dip angle and direction	Slip Rate/Year inches (mm)	Approx. Maximum Magnitude (Mmax)
Anacapa-Dume	47 (75)	Reverse/left-lateral oblique; 45 degrees North	0.02 (0.39)	7.5
Big Pine	25 (41)	Left lateral; vertical	0.02 (0.39)	6.9
Channel Islands thrust	39 (63)	Reverse; 17 degrees North	0.06 (1.5)	7.5
Chino – Central Avenue	17 (28)	Right lateral/reverse oblique; 65 degrees Southwest	0.04 (1)	6.7
Clamshell – Sawpit	10 (16)	Reverse; 45 degrees Northwest	0.02 (0.39)	6.5
Cleghorn	16 (25)	Left lateral; vertical	0.02 (0.45)	6.5
Compton thrust	24 (39)	Reverse; 20 degrees Northeast	0.04 (0.9)	6.8
Cucamonga	17 (28)	Reverse; 45 degrees North	0.06 (1.5)	6.9
Elsinore – Glen Ivy	22 (36)	Right lateral; vertical	0.2 (5)	6.8
Garlock (West)	61 (98)	Left lateral; vertical	0.3 (7.6)	7.3
Hollywood	11 (17)	Reverse/left-lateral oblique; 70 degrees North	0.04 (0.9)	6.4
Holser	12 (20)	Reverse; 65 degrees South	0.02 (0.4)	6.5
Malibu Coast	23 (37)	Reverse/left-lateral oblique; 75 degrees North	0.01 (0.3)	6.7
Mission Ridge – Arroyo Parida – Santa Ana	43 (69)	Reverse; 60 degrees North	0.04 (0.9)	7.2
Newport – Inglewood (Los Angeles Basin)	41 (66)	Right lateral; vertical	0.04 (1)	7.1
Newport – Inglewood (Offshore)	41 (66)	Right lateral; vertical	0.04 (1)	7.1
North Frontal fault zone (West)	32 (51)	Reverse; 45 degrees South	0.004 (0.1)	7.2

Fault Name	Fault Length miles (km)	Fault Type with dip angle and direction	Slip Rate/Year inches (mm)	Approx. Maximum Magnitude (Mmax)
Northridge	19 (31)	Reverse; 42 degrees South	0.06 (1.5)	7.0
Oak Ridge (Onshore)	30 (49)	Reverse; 65 degrees South	0.16 (4)	7.0
Oak Ridge (blind thrust – Offshore)	24 (39)	Reverse; 30 degrees South	0.12 (3)	7.1
Palos Verdes	60 (96)	Right lateral; vertical	0.12 (3)	7.3
Pleito thrust	27 (44)	Reverse; 65 degrees South	0.08 (2)	7.0
Puente Hills (blind thrust)	27 (44)	Reverse; 27 degrees North	0.04 (0.9)	7.1
Raymond	14 (23)	Reverse/left-lateral oblique; 75 degrees North	0.08 (2)	6.5
Red Mountain	24 (39)	Reverse; 60 degrees North	0.08 (2)	7.0
San Andreas (Coachella)	60 (96)	Right lateral; vertical	0.79 (20)	7.2
San Andreas (San Bernardino)	64 (103)	Right lateral; vertical	0.75 (19)	7.5
San Andreas (Mojave)	64 (103)	Right lateral; vertical	1.34 (34)	7.4
San Andreas (Carrizo)	91 (146)	Right lateral; vertical	1.34 (34)	7.4
San Cayetano	26 (42)	Reverse; 60 degrees North	0.24 (6)	7.0
San Gabriel	45 (72)	Right lateral; vertical	0.02 (0.39)	7.2
San Jacinto (San Bernardino)	22 (36)	Right lateral; vertical	0.24 (6)	6.7
San Jose	12 (20)	Reverse/left-lateral oblique; 75 degrees Northwest	0.02 (0.39)	6.4
Santa Monica	17 (28)	Reverse/left-lateral oblique; 75 degrees North	0.04 (1)	6.6
Santa Susana	17 (27)	Reverse; 55 degrees North	0.24 (6)	6.7
Santa Ynez (East)	42 (68)	Left lateral; vertical	0.08 (2)	7.1
Sierra Madre (Sunland)	35 (57)	Reverse; 55 degrees North	0.08 (2)	7.2
Sierra Madre (San Fernando)	11 (18)	Reverse; 45 degrees North	0.08 (2)	6.7
Simi – Santa Rosa	25 (40)	Reverse/left-lateral oblique; 60 degrees North	0.03 (0.7)	7.0
Upper Elysian Park Thrust	12 (20)	Reverse; 50 degrees Northeast	0.07 (1.9)	6.4
Ventura – Pitas Point	25 (40)	Reverse/left-lateral oblique; 75 degrees North	0.06 (1.6)	6.9

Fault Name	Fault Length miles (km)	Fault Type with dip angle and direction	Slip Rate/Year inches (mm)	Approx. Maximum Magnitude (Mmax)
Verdugo	18 (29)	Reverse; 45 degrees Northeast	0.02 (0.39)	6.9
Whittier	24 (38)	Reverse/right-lateral oblique; 75 degrees North	0.1 (2.5)	6.8

Source:
Slip Rate - Dawson, T.E., and R.J. Weldon. 2013. Appendix B – Geologic Slip Rate Data and Geologic Deformation Model in Field, et al. 2013. Uniform California earthquake rupture forecast, version 3 (UCERF3)—The time-independent model: U.S. Geological Survey (USGS) Open-File Report 2013–1165, and California Geological Survey (CGS) Special Report 228.
All Other data - Cao, T. W.A. Bryant, B. Rowshandel, D. Branum, and C.J. Wills. 2003. The Revised California Probabilistic Seismic Hazard Maps, June 2003: California Geological Survey (CGS), available at: http://www.conservation.ca.gov/cgs.

The proposed alignments, SR-14, E1 and E2 intersect numerous faults within the Study Area. A majority of these faults are not active and in accordance with TM 2.9.3 and TM 2.10.6 are considered a "non-hazardous fault zone" (NHFZ). The fault screening process outlined in TM 2.9.3 and TM 2.10.6 is based on the fault's recency of movement and rate of activity (e.g., slip rate and/or recurrence interval) as indicated:

- Hazardous fault zone (HFZ): A fault or fault zone with a recurrence interval ≤1,000 years and/or slip rate ≥1 millimeter/year;
- Potentially hazardous fault zone (PHFZ): Faults with documented evidence of Holocene (11,000 years) activity, or for which Holocene activity is suspected or cannot be reasonably disputed; and
- Non-hazardous fault zone (NHFZ): Faults that are assessed to be older than Holocene.

There are many NHFZ faults within the Study Area; although sympathetic movement could occur along them, their effect on local geologic conditions and hydrogeology (i.e., interconnected fracture networks) is of higher importance for tunnel design. The NHFZ faults include; Agua Dulce, Pole Canyon, Oak Spring, Magic Mountain, Lonetree, Transmission Line, Laurel Canyon, Goose Berry Canyon, Bad Canyon, Mendenhall, and Slaughter Canyon faults (Figure A.5). There have been no geologic slip rates published for these NHFZ faults. They are not included in the USGS Quaternary fault and fold database (USGS and CGS, 2006), none are included in the UCERF3 source model (Dawson and Weldon, 2013), and none have been investigated by the CGS for designation as an Alquist-Priolo Earthquake Fault Zones (Bryant and Hart, 2007). The timing of most recent movement on these faults is not well constrained in previous studies. Carter (1980a) describes various senses of slip for these faults, ranging from right- and left-lateral to dip-slip with left-lateral slip being the dominant sense. Based on existing mapping, the youngest unit offset by any of these faults is Cretaceous granite. Carter (1980a) suggests the faults are not Holocene, but could be as young as late Quaternary. Field observations by Carter (1980a) along the Transmission Line fault reveal evidence of latest activity to be early to middle Pleistocene activity, with faulting observed at the base of old alluvial deposits elevated well above modern drainages incising these deposits and underlying crystalline bedrock. There are no relevant age-dating of the Quaternary deposits along the Transmission Line fault that would help evaluate its age. Furthermore, the Transmission Line fault displaces the Lonetree fault by about four miles left-lateral slip.

Three fault zones, San Gabriel fault, and the Sunland and San Fernando fault splays of Sierra Madre fault zone are active faults and for tunnel design purposes are considered as HFZ. Specific fault information, such as fault displacement and direction of movement is provided in Table 2-2 "San Gabriel Mountain Active Fault Zone Characteristics and Published Displacement Potential." The information provided in Table 2-2 is summarized from two CHSR project documents TM 2.10.6, "Fault Hazard Analysis and Mitigation Guidelines, R1" (2014), and "Engineering Report 15% Draft Fault Hazard Evaluation Report" (2015a) and several published reports, where referenced.

The San Gabriel Fault Zone extends 45 miles (72 kilometers) northwest, bisecting portions of the San Gabriel Mountains, Santa Clarita Valley, and Sierra Pelona Mountains. During earlier phases of the transition from a convergent to a transform plate boundary in the Miocene, the San Gabriel Fault Zone was the primary plate boundary structure and accumulated total right-lateral displacement of about 25 – 47 miles (40 – 75 kilometers) (Powell et al., 1993; Crowell, 2003).

The northwest-striking San Gabriel Fault Zone generally dips steeply east to vertical near the surface in the Honor Rancho and Saugus oil fields in the Santa Clarita Valley. Based on oil well logs, they note that at depth, the fault dip locally decreases to as shallow as about 60 degrees northeast in the Saugus oil field. Through the mountains, the fault cuts across rugged topography with a relatively linear strike indicating a near vertical dip. The UCERF3 model assigns a dip of 61 degrees northeast (Field et al., 2013). Estimates of slip rate vary markedly along strike of the SGFZ, with the highest rates of activity observed along the southern half of the northern section. Both right-lateral and reverse components of slip have been recognized. On the basis of geomorphology associated with the fault, its estimated a lateral slip rate of less than 1 millimeter/year (0.039 inches/year). Geologic cross-sections constrained by oil well data in the Saugus oil field suggest a reverse dip-slip rate of 2.5 to 3.0 millimeter/year (0.98 – 0.12 inches/year). The USGS Quaternary fault and fold database (USGS and CGS, 2006) assigns the fault to the second lowest slip rate category of 0.2 to 1 millimeter/year (0.008 – 0.039 inches/year). For the UCERF3 characterization, Dawson and Weldon (2013) recalculated a horizontal slip rate of 0.2 to 1.0 millimeter/year, (0.008 – 0.039 inches/year) and a dip-slip rate of 2.5 to 3.0 millimeter/year (0.98 – 0.12 inches/year) for the northern section of the fault. The UCERF3 model employs a geologic, purely right-lateral slip rate of 0.39 millimeter/year, or 0.02 inches/year (Dawson and Weldon, 2013).

The Sierra Madre fault zone (Sunland fault) extends 35 miles (57 kilometers) northwest, bisecting portions of the high range front of the western San Gabriel Mountains. This fault zone accommodates primarily compression associated with the Transverse Ranges (Crook et al., 1987).The Sunland fault is generally considered to dip approximately 50 to 55 degrees northeast and to extend from the ground surface to approximately 16 kilometers depth (Heaton, 1982). The fault trace and geomorphic expression of the Sunland fault east of Big Tujunga Canyon is relatively linear and far less complex than that of the western end, which forms arcuate geometries that trend up into northeast-oriented drainages. Little is understood of the down-dip geometry of the Sunland fault due to a lack of subsurface data. The UCERF3 model assigns a north dip of 53 degrees and depth of 14.2 kilometers (Field et al., 2013).

Several slip rate estimates have been developed for Sunland fault. Based on measurements of dip-slip displacement in trench exposures, Rubin et al. (1998) estimate a Holocene dip-slip rate of about 0.6 millimeters/year (0.2 inches/year) for the Sunland fault. An alternative, and longer-term, slip rate of 2.2 millimeters/year (0.9 inches/year) (SCEC Working Group C, 2001). The USGS Quaternary fault and fold database (USGS and CGS, 2006) assigns the Sunland fault, to its second highest slip rate category, 1 to 5 millimeters/year (0.039 – 0.2 inches/year). The UCERF3 source model utilizes a purely reverse geologic slip rate of 1 to 3 millimeters/year (0.039 – 0.12 inches/year), with a best estimate of 2 millimeters/year (0.08 inches/year) (Dawson and Weldon, 2013) based on the work of Crook et al. (1987).

The San Fernando fault extends 11 miles (18 kilometers) northwest along the base of the San Gabriel Mountains adjacent to Tujunga Wash and San Fernando Valley. The San Fernando fault, which is part of the much larger Sierra Madre fault system, was the causative fault for the 1971 M6.6 Sylmar earthquake. The fault, which accommodates compression in the northern San Fernando Valley, has been subdivided into several sections based on the unique surface rupture characteristics displayed during the 1971 earthquake (Barrows et.al., 1974). The most commonly observed names are, from west to east, the Mission Wells, Sylmar, Tujunga, and Lakeview sections.

The San Fernando fault generally strikes west-northwest and is interpreted to dip about 40 degrees to 50 degrees northeast along much of its trace (Heaton, 1982) within the Project area. Based on aftershock imaging of the 1971 earthquake, the fault extends to about 13 to 15 kilometers (8-9 miles) depth. The UCERF3 source model assigns a 45° north dip, and depth of 13.0 kilometers (eight miles) along the fault plane.

Slip rate estimates for the San Fernando fault and other unnamed fault scarps are derived from scarp heights and age estimates of offset alluvial surfaces near Pacoima Wash. Previous studies (Lindvall and Rubin, 2003) identified terraces in Pacoima Wash that have been uplifted along three south-facing scarps and used cosmogenic radioisotope dating methods to calculate a dip-slip rate of 1.2 millimeters/year (0.05 inches/year). The San Fernando fault zone is assigned to the 1 to 5 millimeters/year (0.039 – 0.2 inches/year) in the USGS Quaternary fault and fold database (USGS and CGS, 2006). Also similar, the UCERF3 source model assigns the fault a purely reverse geologic slip rate of 1 to 3 millimeters/year (0.039 – 0.12 inches/year), with a best estimate of 2 millimeters/year (0.08 inches/year) (Dawson and Weldon, 2013) based on the work of Lindvall and Rubin (2003).

Site-specific fault characteristics are provided in Table 2-2 (San Gabriel Mountain Active Fault Zone Characteristics and Published Displacement Potential) for the San Gabriel, Sunland and San Fernando faults as compiled from HSRA documents. Along with specific fault information, such as fault displacement and direction of movement, the table includes data on the angle of the tunnel alignment's intersection with the fault and alignment's station interval affected.

Table 2-2 San Gabriel Mountain Active Fault Zone Characteristics and Displacement

Name of Fault Zone (Fault Splay)	Fault Strike (Azimuth)	Fault Dip	Alignments Crossed	Approximate Intersection Angle Between Fault Zone and Alignment	Approximate Station Interval at Intersection with Tunnel Invert	Alignment Width Within Fault Zone (feet)	Number of Splays in Fault Zone	Horizontal Displacement (feet)	Horizontal-to-Vertical Slip Component Ratio	Approximate Vertical Displacement (feet)	Direction of Horizontal Displacement	Direction of Vertical Displacement during Earthquake
San Gabriel Fault	295°	61°NE	SR-14	60°	1546+00 to 1610+00	6,400	5	4.9	7 to 1	0.7	Right-lateral	North side up
			E1	50°-70°	1500+00 to 1522+00	2,175	4	4.9		0.7		
			E2	±90°	1362+00 to 1425+00	6,225	7	4.9		0.7		
Sierra Madre Fault (Sunland, Lopez and Hospital fault splays)	295°	55°NE	SR-14	±90°	1716+00 to 1738+00	2,200	2	3.6	1 to 1.5	5.4	Left-lateral	North side up
			E1	±90°	1616+00 to 1622+00	600	2	3.6		5.4		
			E2	±90°	1538+00 to 1556+00	1,800	3	3.6		5.4		
Sierra Madre Fault (San Fernando splay)	285°	45°NE	SR-14	±90°	1832+00 to 1872+00	4,000	>5	5.6	1.5 to 1	3.7	Left-lateral	North side up
			E1	±90°	1722+00 to 1762+00	4,000	>5	5.6		3.7		
			E2	±90°	1617+00 to 1632+00	1,500	>5	5.6		3.7		

Source:
Fault Location - Campbell, R.H., C.J. Willis, P.J. Irvine, and B.J. Swanson. 2014. *Preliminary Geologic Map of the Los Angeles 30'x60' Quadrangle, California*, version 2.1: California Geological Survey, Scale 1:100,000.
United States Geological Survey (USGS) and California Geological Survey (CGS). 2006. Quaternary Fault and Fold Database for the United States. Accessed September 28, 2016 from USGS website: http//earthquakes.usgs.gov/hazards/qfaults/
Fault Displacement and Ratios - Tables A-3 and A-4 from, California High-Speed Rail Authority (Authority). 2015a. *Engineering Report, 15% Draft Palmdale to Burbank, Fault Hazard Evaluation Report.* Prepared by HMM/URS/Arup RC, dated June 2015

2.6 Local Geology

The project Study Area is generally located in the western San Gabriel Mountains and specifically within the Angeles National Forest (ANF). The local geology of the project Study Area is complex due to multiple stages of metamorphism, igneous intrusion, rotation, and subsequent uplift and faulting of the area over the past 1.7 billion years. Previous mapping of the San Gabriel Mountains by the CGS (Campbell et al., 2014) and the USGS (Yerkes and Campbell, 2005) provided the surface mapping of the Study Area's geology. To supplement this existing data and check site-specific geologic information, limited geologic mapping and a subsurface investigation was conducted within the project area. The subsurface investigation included drilling, collecting core and performing geophysical and hydrogeological downhole tests. Detail descriptions of the field activities, including geologic mapping and coring, are provided in Section 3.

Geology maps and profiles showing anticipated subsurface geology along each of the tunnel alignments within the ANF were compiled from published data. The geologic map, plans and profiles are provided in Appendices A.5 (Local Geologic Map), A.6 (SR-14 Geologic Plan and Profile), A.7 (E1 Geologic Plan and Profile), and A.8 (E2 Geologic Plan and Profile). Geologic descriptions of rock formations and lithology were modified based on site-specific information; however, they generally follow the nomenclature set forth by surface mapping performed by CGS (Campbell et.al. 2014) and the geologic research performed by Carter (1980a).

The rocks within the project Study Area include metamorphic and igneous rocks with layers of sedimentary rocks mantling the northwestern and southern edges of the mountains. The metamorphic and igneous rocks include remnants of Proterozoic gneiss that have been intruded by a Proterozoic anorthosite-gabbro complex, the Mount Lowe Granodiorite (intrusive suite) of Permian-Triassic age, Mesozoic granitic (including the Mount Josephine granodiorite) and gneissic rocks. The oldest and one of the most distinctive rocks on the Study Area is the approximately 1.7 billion year old Mendenhall Gneiss. The Mendenhall Gneiss was described and named by Oakeshott (1958). This gneiss is exposed in the Project area north of the San Gabriel fault and south of the anorthosite-gabbro complex (Figure A.5). It was subjected to high temperature metamorphism 1.2 billion years ago and in many areas again during the Mesozoic (Silver, 1971; Ehlig, 1975b). The structurally complex unit of anorthosite-gabbro and related rocks are exposed over an area of about 80 square miles, mostly in the Study Area. The anorthosite-gabbro complex is described in detail by Carter (1980a, 1980b and 1982) and Oakeshott (1958). The blue-gray to white andesine anorthosite is the most abundant rock type in the anorthosite-gabbro complex (Carter, 1980a) with the gabbro the next most abundant followed by the syenite. This igneous complex was emplaced 1.22 billion years ago (Silver, 1971; and Carter, 1980a). Studies by Carter (1980a) indicate the complex was initially stratiform with prominent compositional layering produced by gravitational settling of crystals. The structure has subsequently become geologically complex due to several episodes of deformation and faulting. These rocks are generally coarse grained and have unusual textures. These rocks were encountered in the current subsurface explorations and a more detailed description is provided in Section 5.1.

The Mount Lowe Granodiorite crops out in the northeastern part of the project Study Area and is composed of a medium- to coarse-grained diorite and quartz diorite. Granitic intrusions into the Mount Lowe Granodiorite are rare in the area, although common in the eastern part of the San Gabriel Mountains (Ehlig, 1975b). The age of this predominantly white rock is approximately 220 million years old. Metamorphosed dikes derived from basalt and andesite are common in the Mount Lowe Granodiorite and older rock units. Younger Mesozoic-age granitic rocks, ranging from quartz diorite to granite in composition have intruded all other older rock units. The Cretaceous-age Mount Josephine Granodiorite is the largest part of the Mesozoic intrusion. In the project area, this unit is generally located south of the San Gabriel fault. Mount Josephine Granodiorite was encountered in cores retrieved from two of the borings from the current subsurface investigation, ALT-B2 and ALT-B3.

Northwest and south of the metamorphic and igneous rock outcrops are layers of Tertiary-age sedimentary rocks. The sedimentary deposits have been both faulted against and deposited over the metamorphic and igneous rocks. In the northwest part of the Study Area, the sedimentary layers belonging to the Vasquez, Tick and Mint Canyon Formations have been deposited. The Vasquez Formation is Oligocene to early Miocene in age and includes sandstone, mudstone, and conglomerate with interbedded andesite-basalt. The Vasquez Formation is greater than 12,000 feet thick and rests on crystalline bedrock. Overlaying the Vasquez formation is the Miocene Tick Canyon Formation, which is comprised of well-cemented conglomerate sandstone, claystone and siltstone of fluvial origin (Oakeshott, 1958). The Tick Canyon is early to middle Miocene in age. Deposited above the Tick Canyon Formation is the Mint Canyon Formation. The Mint Canyon Formation is middle to late Miocene in age (Campbell et.al. 2014) and includes semi-consolidated nonmarine layers of arkosic and conglomerate sandstone, siltstone, mudstone, and an interbedded tuff near the top of the formation. The formation is fossiliferous and approximately 2,500 feet thick.

In the southern part of the Study Area, the sedimentary layers belonging to the Modelo, Towsley and Saugus Formations are present. The Modelo Formation is middle to late Miocene in age and consists of layers of thinly-bedded mudstone, diatomaceous shale, siltstone with interbeds of sandstone. Its thickness varies by location, but overall can easily exceed 10,000 feet. Deposited above the Modelo Formation is the late Miocene to early Pliocene Towsley Formation. The Towsley Formation consists of interbedded marine siltstone, mudstone, sandstone and conglomerate layers. Fossils indicate the Towsley Formation was deposited in water in excess of 600 feet deep. The unit has a maximum thickness of approximately 4,000 feet, and is overlain by the Saugus Formation. The Saugus Formation is a non-marine unit that is Pliocene to Pleistocene in age. The Saugus Formation, which contains layers of sandstone, sandy conglomerate, and siltstone, may be up to 12,000 feet thick. The unit is weakly to moderately cemented.

Above the bedrock, units include surficial deposits of landslide debris and alluvium (old and young). In the Study Area these deposits are generally found along canyon bottoms (alluvium) and along steep canyon walls (landslide debris). These surficial deposits have been included on the geology maps found in Appendices A.5, A.6, A.7, and A.8. However, the proposed alignments within the ANF will be primarily in tunnel below the ground surface. These surficial deposits should not impact tunnel design.

Summaries of the geologic units and their anticipated locations are presented in Table 2-3 Summary of Local Geologic Units along SR-14 Alignment Shown in Figure A.6, and Table 2-4 Summary of Local Geologic Units along E1 Alignment Shown in Figure A.7, and Table 2-5 Summary of Local Geologic Units along E2 Alignment Shown in Figure A.8.

Table 2-3 Summary of Local Geologic Units Along SR-14 Alignment Shown on Figure A.6

Formation Name (Map Symbol)	Rock Type	Lithology Description	Approximate Station
Mint Canyon Formation (Tmc, Tmcm, Tmcd)	Non-marine Sedimentary Fluvial and Lacustrine	Middle to late Miocene- Two distinct units (of three); a lower reddish brown rock breccia, sandstone, siltstone and mudstone and upper brownish to greenish siltstone and tuff.	1327+00-1454+00
Vasquez Formation (Tvz, Tvzc, Tvzs, Tvzb, Tvza)	Non-marine Sedimentary and Volcanic	Oligocene to early Miocene to - Yellowish and reddish sandstone, conglomerate and interbedded andesite-basalt. Overlies Pre-Tertiary crystalline basement rocks, unconformably underlies Tick Canyon Formation. Includes numerous beds and lenses of megabreccia, many monolithologic	1454+00-1488+00 [may encounter Tvz 1398+00-1414+00 and 1496+00-1498+00 (depending on unit thickness and dip of bedding).]

Formation Name (Map Symbol)	Rock Type	Lithology Description	Approximate Station
Cretaceous Granitic (Kgr) Mount Josephine Granodiorite (Kgrd)	Plutonic Igneous	Cretaceous- Kgr: Granitic Rocks include; quartz monzonite, and granodiorite to tonalite, quartz diorite; chiefly quartz diorite. Kgrd: Granodiorite and related rocks includes; gray medium to coarse-grained granodiorite, quartz diorite and granite. Large inclusions and pendants of gneiss and Placerita metasediments present. Commonly gneissoid near contacts with older rocks.	1606+00-1705+00
Anorthosite-Gabbro Complex (Pan, Psy, Pfgb, Plgb, Pjgb, Pjgba, Pgbla, Pgb)	Plutonic Igneous with metamorphic gneiss	Proterozoic- Anorthosite (Pan), syenite (Psy), ferro-gabbro (Pfgb), leucogabbro (Plgb), jotunitic gabbro (Pjgb), jotunite-norite-gabbro-diorite (Pjgba), anorthosite inclusion-rich gabbro (Pgbla), gabbro (Pgb)	1488+00-1569+00
Mendenhall Gneiss (Pmgn)	Metamorphic	Proterozoic- Layered migmatitic felsic gneiss and mafic granulite, rare interlayered augen gneiss and aluminous gneiss	1569+00-1606+00

Source: Campbell, R.H., C.J. Willis, P.J. Irvine, and B.J. Swanson. 2014. *Preliminary Geologic Map of the Los Angeles 30'x60' Quadrangle, California*, version 2.1: California Geological Survey (CGS), Scale 1:100,000.

Table 2-4 Summary of Local Geologic Units Along E1 Alignment Shown on Figure A.7

Formation Name (Map Symbol)	Rock Type	Lithology Description	Approximate Station
Saugus Formation (QTs)	Non-marine sedimentary	Late Pleistocene to late Pliocene- light gray to yellowish-gray sandstone and pebble conglomerate, slightly consolidated, weakly to moderately cemented. Commonly cross-bedded and channeled. Formed in transitional fluvial-alluvial fan environments	1620+00-1623+00
Juncal Formation (Tj) [Former Martinez Formation]	Marine Sedimentary	Late early Eocene- Coarse-grained greenish-black to light olive gray sandstone with thin interbeds of black shale and lenticular beds of conglomerate. Clasts include purple volcanic porphyry and local large siltstone rip-up clasts. Formed in middle to upper submarine fan turbidity currents Observed in Elsmere Canyon as thin fault bounded slivers within the San Gabriel Fault Zone.	1514+00-1515+00
Cretaceous Granitic (Kgr) Mount Josephine Granodiorite (Kgrd)	Plutonic Igneous	Cretaceous- Kgr: Granitic Rocks include; quartz monzonite, and granodiorite to tonalite, quartz diorite; chiefly quartz diorite. Kgrd: Granodiorite and related rocks includes; gray medium to coarse-grained granodiorite, quartz diorite and granite. Large inclusions and pendants of gneiss and Placerita metasediments present. Commonly gneissoid near contacts with older rocks.	759+00-786+00 (Kgr) 793+00-806+00 (Kgr) 1502+00-1575+00 (Kgrd) 1601+00-1620+00 (Kgrd)
Diorite Gneiss (Mzdg)	Metamorphic	Early to middle Mesozoic- Dark colored gneiss including metadiorites, massive hornblende diorite and amphibolite and biotite schists; intrudes Placerita Formation and is intruded by Cretaceous-age granitic rocks.	1575+00-1601+00
Mount Lowe Granodiorite (Intrusive Suite) (TRlgd, TRlgdh, TRlgdp, TRhdg, TRlgb, TRlgdb, TRlb, TRlh)	Plutonic Igneous - Layered Pluton with metamorphic ambhiolite facies rocks.	Triassic- Hornblende diorite, quartz diorite near the base of pluton; albite-rich granite and syenite in upper portion of pluton. Metamorphic grade varies with proximity to Cretaceous intrusive rocks. Pluton is rich in plagioclase.	679+00-723+00 (TRhdg), 750+00-759+00 (TRhdg), 786+00-793+00 (TRhdg) 806+00-858+00 (TRlgdp)
Gneiss (Pgn)	Metamorphic	Proterozoic- Alternating discontinuous dark brown biotite-rich and light-colored quartz-feldspar-rich layers.	942+00-973+00

Formation Name (Map Symbol)	Rock Type	Lithology Description	Approximate Station
Anorthosite-Gabbro Complex (Pan, Psy, Pfgb, Plgb, Pjgb, Pjgba, Pgbla, Pgb)	Plutonic Igneous with metamorphic gneiss	Proterozoic- Anorthosite (Pan), syenite (Psy), ferro-gabbro (Pfgb), leucogabbro (Plgb), jotunitic gabbro (Pjgb), jotunite-norite-gabbro-diorite (Pjgba), anorthosite inclusion-rich gabbro (Pgbla), gabbro (Pgb)	916+00-942+00 (Pan) 973+00-1290+00 (Pan) 1290+00-1351+00 (Pjgb) 1351+00-1373+00 (Plgb) 1373+00-1409+00 (Pfgb) 1409+00-1455+00 (Pjgb)
Mendenhall Gneiss (Pmgn)	Metamorphic	Proterozoic- Layered migmatitic felsic gneiss and mafic granulite, rare interlayered augen gneiss and aluminous gneiss	1455+00-1502+00

Source: Campbell, R.H., C.J. Willis, P.J. Irvine, and B.J. Swanson. 2014. *Preliminary Geologic Map of the Los Angeles 30'x60' Quadrangle, California*, version 2.1: California Geological Survey (CGS), Scale 1:100,000.

Table 2-5 Summary of Local Geologic Units Along E2 Alignment Shown on Figure A.8

Formation Name (Map Symbol)	Rock Type	Lithology Description	Approximate Station
Saugus Formation (QTs)	Non-marine sedimentary	Late Pleistocene to late Pliocene- light gray to yellowish-gray sandstone and pebble conglomerate, slightly consolidated, weakly to moderately cemented. Commonly cross-bedded and channeled. Formed in transitional fluvial-alluvial fan environments	1417+00-1452+00 1536+00-1580+00
Towsley Formation (Tw)	Marine Sedimentary	Early Pliocene to late Miocene Overlies Modelo Formation (west) and interfingers/overlaps Modelo Formation in the vicinity of the San Fernando Valley. Recognized by a thick pebbly sandstone basal layer, often lenticular, may be turbidity current deposits in a submarine fan.	1580+00-1600+00
Modelo Formation (Tm, Tms)	Marine Sandstone and Conglomerate	Late to middle Miocene Predominantly thin-bedded mudstone, diatomaceous shale, and siltstone with interbeds of very fine-grained to coarse-grained sandstone. Turbidite features indicate submarine fan deposition (Sullwold, 1960)	1536+00-1551+00 1600+00-1625+00
Cretaceous Granitic (Kgr) Mount Josephine Granodiorite (Kgrd)	Plutonic Igneous	Cretaceous- Kgr: Granitic Rocks include; quartz monzonite, and granodiorite to tonalite, quartz diorite; chiefly quartz diorite. Kgrd: Granodiorite and related rocks includes; gray medium to coarse-grained granodiorite, quartz diorite and granite. Large inclusions and pendants of gneiss and Placerita metasediments present. Commonly gneissoid near contacts with older rocks.	759+00-786+00 (Kgr) 793+00-806+00 (Kgr) 1376+00-1389+00 (Kgrd) 1394+00-1408+00 (Kgrd) 1452+00-1536+00 (Kgrd)

Formation Name (Map Symbol)	Rock Type	Lithology Description	Approximate Station
Diorite Gneiss (Mzdg)	Metamorphic	Early to middle Mesozoic- Dark colored gneiss including metadiorites, massive hornblende diorite and amphibolite and biotite schists; intrudes Placerita Formation and is intruded by Cretaceous-age granitic rocks.	1408+00-1417+00
Mount Lowe Granodiorite (Intrusive Suite) (TRlgd, TRlgdh, TRlgdp, TRhdg, TRlgb, TRlgdb, TRlb, TRlh)	Plutonic Igneous - Layered Pluton with metamorphic ambhiolite facies rocks.	Triassic- Hornblende diorite, quartz diorite near the base of pluton; albite-rich granite and syenite in upper portion of pluton. Metamorphic grade varies with proximity to Cretaceous intrusive rocks. Pluton is rich in plagioclase.	679+00-723+00 (TRhdg), 750+00-759+00 (TRhdg), 786+00-793+00 (TRhdg) 806+00-858+00 (TRlgdp)
Gneiss (Pgn)	Metamorphic	Proterozoic- Alternating discontinuous dark brown biotite-rich and light-colored quartz-feldspar-rich layers.	942+00-973+00
Anorthosite-Gabbro Complex (Pan, Psy, Pfgb, Plgb, Pjgb, Pjgba, Pgbla, Pgb)	Plutonic Igneous with metamorphic gneiss	Proterozoic- Anorthosite (Pan), syenite (Psy), ferro-gabbro (Pfgb), leucogabbro (Plgb), jotunitic gabbro (Pjgb), jotunite-norite-gabbro-diorite (Pjgba), anorthosite inclusion-rich gabbro (Pgbla), gabbro (Pgb)	916+00-942+00 (Pan) 973+00-1099+00 (Pan) 1099+00-1108+00 (Psy) 1108+00-1127+00 (Pjgba) 1127+00-1154+00 (Pjgb) 1154+00-1169+00 (Pjgba) 1169+00-1357+00 (Pjgb)
Mendenhall Gneiss (Pmgn)	Metamorphic Rocks	Proterozoic- Layered migmatitic felsic gneiss and mafic granulite, rare interlayered augen gneiss and aluminous gneiss	1357+00-1376+00 1389+00-1394+00

Source: Campbell, R.H., C.J. Willis, P.J. Irvine, and B.J. Swanson. 2014. *Preliminary Geologic Map of the Los Angeles 30'x60' Quadrangle, California*, version 2.1: California Geological Survey (CGS), Scale 1:100,000.

2.7 Hydrogeology

The hydrogeology of the project Study Area is dominated by water flow along fractures in the bedrock terrain of the mountains. The igneous and metamorphic bedrock comprising the majority of the project area contains little to no porosity within the rock mass in which groundwater could reside. However, the mountains have been subjected to numerous episodes of deformation, including faulting and uplift, which has fractured the bedrock. This fracturing and faulting has created fissures within the bedrock that allows groundwater to reside and move through the rock mass along preferred fracture systems. As the water is stored in the fractured bedrock it will move down through fractures (and faults) if the fractures are interconnected and have sufficient capacity to accommodate the water volume. If the water-laden fracture/fault intersects a canyon wall, the groundwater will discharge at the ground surface as a spring or seep and join with surface runoff in the canyon's stream. The combined spring water and surface runoff water will flow in the canyon as ephemeral stream flow and percolate into canyon bottom if alluvium present. Here the combined subsurface and intermittent surface water flow will possibly recharge local water-bearing alluvium to the west, north, and south of the project Study Area.

If the water movement in the fractures intersects a less permeable rock mass or a fault along its path, the groundwater movement could be interrupted and redirected, perched or held behind the fault acting as a barrier to the groundwater flow.

The hydrogeology of the project area is not very well known because there has been very little information available to characterize the groundwater behavior. The data collected through this study is essential for understanding the behavior of groundwater within the western San Gabriel Mountains. Currently the project field investigation has collected groundwater data from five widely-spaced core holes. The information collected and the interim results include: groundwater chemistry testing (Sections 4.3, 5.5 and 5.6), in-situ hydraulic conductivity (Section 5.5 and Appendix H), and groundwater pressure monitoring (Section 5.2).

Supplementing the field data from the core holes are the data from groundwater monitoring of water wells, springs and seeps within the San Gabriel Mountains hard rock aquifer by the USGS (Davis and Shelton, 2014). This groundwater monitoring is part of joint effort between the USGS and the California State Water Resources Control Board for the California Groundwater Ambient Monitoring and Assessment (GAMA) Program. The GAMA program is designed to provide unbiased assessment of untreated, shallow groundwater quality, with its main goal to improve groundwater monitoring and to increase the availability of groundwater-quality data to the public. Within the Study Area, the GAMA program collected groundwater from three wells and one spring between March 2011 to March 2012. The groundwater collected during the GAMA program was tested for; standard field water-quality parameters, volatile organic compounds, pesticides, perchlorate, inorganic constituents (ions, nutrients, dissolved solids, arsenic, chromium, iron, etc.), and radioactive constituents (tritium, radon, uranium isotopes, carbon-14). The current subsurface investigation tested groundwater from the five core holes for many of the GAMA parameters in order to maintain consistency between the two test programs. This will allow for a better understanding of groundwater conditions and possibly geologic structure of the Study Area. Generally, the groundwater chemistry from the core holes was similar to that reported by the GAMA program. That is, the constituent detections (and concentrations) and constituent non-detections of the general parameters between the core holes and the GAMA wells/spring were similar. Additional information for the groundwater sampling results can be found in Section 3.5.

In addition to the data from the core holes testing and the GAMA data on wells and springs, a field survey of known springs and seeps within the ANF is being conducted. Based on the USGS Hydrography Dataset and topographical maps of the area, currently sixteen spring/seep locations have been identified (Figure A.9). Future monitoring of these locations are planned to collect, if possible, a sufficient volume of water for detailed laboratory testing. The laboratory testing parameters of the spring water will be the same as the testing parameters for the groundwater samples collected from the core holes, discussed in Section 4.3. The evaluation of the general chemistry of the core hole and spring water may allow for comparison of their source and/or possible connection between surface water and deep groundwater at the depth of the proposed tunnels. Results of the springs and seeps monitoring will be presented in a separate, future report.

3 FIELD INVESTIGATIONS

The geotechnical investigation (GI) program included limited reconnaissance (surface) geologic mapping and drilling five rock core borings within the ANF. Figures referenced in this section are included in Appendix B.

3.1 Reconnaissance Geologic Mapping

Limited reconnaissance level geologic mapping was performed to “ground truth” geologic information presented in published sources that was referenced as an aid to evaluating potential core hole locations. The Geologic mapping included traverses along Kagel Canyon truck trail and several drainages between Kagel Canyon truck trail and Little Tujunga Canyon Rd.; along Mendenhall Truck Trail north of Dillon Divide (Appendix A).

During the reconnaissance geologic mapping, observations and measurements were made that included the strike and dip of joints, shears, and other discontinuities within the exposed bedrock. The locations of observable traces of faults were compared to the published sources to refine and modify the geologic exploration plan.

3.2 Rock Core Borings

The purposes of the rock core borings were: 1) obtain a continuous log of the rock lithology and rock mass characteristics; 2) develop geologic structural interpretation; 3) retrieve rock samples for laboratory testing; 4) access the sub-surface for in situ geophysical logging and in-situ hydraulic testing; and 5) install instrumentation for groundwater monitoring. A pre-qualified drilling subcontractor provided rock coring equipment and drilling services and obtained and supplied potable water for drilling operations. The drilling subcontractor utilized triple tube wireline rock core drilling methods to obtain continuous HQ (2.4-inch diameter) core samples at each rock core boring location. Drilling methods were in general accordance with ASTM D2113, Standard Practice for Rock Core Drilling and Sampling of Rock for Site Investigation (ASTM, 2016). Helicopter support was used for Core Holes FS-B1 and E1-B1. Appendix C presents more information regarding site-specific drilling conditions, equipment, and operations for each boring.

Appendix A shows the locations of the rock core borings. Table 3-1 summarizes the rock core boring locations. Appendix D presents core boring logs and digital photographs of the rock core boxes.

Table 3-1 Summary of Rock Core Borings

Core Hole	Northing Easting[1]	Surface Elevation[1]	Mean Azimuth[2]	Mean Plunge[3]	Total Core Depth[4]	Termination Elevation[5]
	feet		degrees		feet	
FS-B1	1,964,046.01 6,484,948.43	4,212.35	322.9	67.1	1,004.7	3,286.8
E1-B1	1,966,444.93 6,478,409.29	4,893.30	275.0	88.6	2,702.7	2,191.4
E1-B2	1,948,078.09 6,456,059.35	2,762.25	001.1	68.1	1,005.9	1,828.9
ALT-B2	1,953,454.77 6,441,306.43	2,835.89	162.7	68.0	1,617.8	1,335.9
ALT-B3	1,950,739.82 6,439,523.76	3,465.45	115.2	87.9	2,100.2	1,366.7

[1] Core hole locations were surveyed by Virtek Company. The horizontal and vertical datums are NAD83 (CCS Zone 5) and NAVD88, respectively.
[2] The azimuth is obtained from the mean orientation as measured from the downhole geophysical surveys performed by GEOVision. The azimuth of near vertical core holes is negligible.
[3] The reported plunge is the boring inclination measured from the horizontal plane and is the mean inclination as measured from the downhole geophysical surveys performed by GEOVision.
[4] The total core depth is referenced from the total number of drill rods used to advance the hole from ground surface along the core axis to hole termination.
[5] The termination elevation is approximated using the mean plunge of the core hole and the total core depth.

Prior to mobilization and drilling within the ANF, a special use permit (SUP) from the USFS and well construction permits from the County of Los Angeles Department of Environmental Health were obtained. Drilling activities began on January 5, 2016 and continued through September 14, 2016. Geotechnical professionals were onsite during drilling to document and oversee the drilling process and conditions; collect, photograph and log the core in the as-received condition within the stainless-steel split liners; label and store core sample in wood core boxes, each holding approximately 15 feet of core; and oversee downhole geophysics, in-situ testing and instrumentation installations, and backfilling. Geotechnical professionals prepared field logs using Caltrans (2010) methods supplemented by methods suggested by the International Society for Rock Mechanics (2015).

Core boxes were transported from the ANF to the project core storage facility located in Valencia. At the core storage facility, geotechnical professionals photographed the rock core (Appendix D), further evaluated the rock core and conducted quality control of the field logs. Geotechnical professionals assigned laboratory testing and prepared the rock core boring logs (Appendix D) in general accordance with the CALTRANS (2010) format using gINT geotechnical software by Bentley Systems (2016). Figure 3-1 through Figure 3-16, which are located in Appendix B of this report, summarize rock core boring data from the gINT database

To characterize the subsurface conditions, descriptions of the rocks and other features within them, such as faults, shears, and joints were recorded on the core boring logs during the drilling operations. Additional discontinuity orientation information was collected during the geophysical surveys after the cores were advanced to the total depth. Select intervals of the core were evaluated through petrographic analysis and laboratory tests to validate field classifications.

The rock descriptions and discontinuity orientation data are used together to assess and define structural domains that share common characteristics. These domains are typically bounded by contacts between rock types, faults, or shear zones within the rock. The domains may share similar tectonic histories but may have been rotated slightly relative to one another during the mountain building process. These differences in rock type or quality and minor rotations cause the orientations and frequency of discontinuities to differ slightly between domains. These differences can have an effect on the geomechanical rock properties.

It should be noted that the locations of the core holes focused on the anorthosite-gabbro body, which comprise the core of the western San Gabriel Mountains; the Transmission Line and San Gabriel Faults, which are significant tectonic features to be crossed by the alignments; and areas of the highest overburden and hydrostatic pressures. A comprehensive study of geologic conditions along a particular tunnel alignment was not performed for this data report.

3.3 Instrumentation

Upon completion of drilling, in-situ testing and performing downhole geophysics, fully-grouted vibrating wire piezometers (VWP) were installed at each rock core boring location to measure ground temperature and groundwater pressure. Fiber optic cables were installed within several core holes as part of a cooperative study with California State University (CSU).

3.3.1 Vibrating Wire Piezometers

VWP are comprised of four to five fully-grouted vibrating wire pressure transducers (VWPT) installed at various intervals of the rock core boring. The VWPT measure the discrete temperature and pressure at select elevations within the rock core boring. Dataloggers are maintained at the core boring locations to collect VWPT readings that are periodically downloaded. Appendix F presents information regarding the VWPT calibration, installation, monitoring and data reduction methods. Table 3-2 summarizes the instrument installations. The groundwater pressures measured from the instruments are presented for comparison with other rock mass properties in Figure 3-1 through Figure 3-16 (Appendix B).

Table 3-2 Summary of Instrumentation Installations

Core Hole	VWPT-1 (Yellow)[1]	VWPT-2 (Orange)[1]	VWPT-3 (Red)[1]	VWPT-4 (Purple)[1]	VWPT-5 (Blue)[1]	Fiber Optic Cable
	Instrumentation Core Depths (feet)					
FS-B1	169.5	397.5	521.5	939.5	NA	No
E1-B1	225.0	1,355.0	1,800.0	2,383.0	2,680.0	Yes
E1-B2	244.0	595.0	726.0	976.0	NA	Yes
ALT-B2	200.0	720.0	968.0	1,125.0	1,575.0	Yes
ALT-B3	502.0	935.0	1,376.0	1,747.0	2,032.0	Yes

[1] Instrument wire colors correspond to actual color-coding of the wires on-site within the instrument vaults.
[2] Intsrument core depths reported are not vertical depths and do not include corrections for core hole plunge.

3.3.2 Fiber Optic Cable

The California High Speed Rail Authority authorized California State University (CSU) to install fiber optic cables within the rock core borings to facilitate additional data collection. The fiber optic cable installation was arranged and coordinated by faculty from CSU Fullerton, and CSU Long Beach. The fiber optic cables allow the measurement of near-continuous ground temperature with depth. The data will be used by students and faculty at those institutions for ongoing research. The CSU data collection and studies are separate from the geotechnical study and are not included in this report.

3.4 Geophysical Investigations

Downhole geophysical logging, which consists of lowering various probes (sondes) into the core hole was performed at each of the core holes to create a near-continuous log of physical rock and fluid properties.

Instability of the core hole precluded data collection within certain zones that presented a high risk of getting the geophysical tool stuck in the core hole. Casing was used to temporarily stabilize the core hole so deeper intervals of the core hole could be logged. The casing prevented data acquisition of intervals that presented an unacceptable level of risk of damage or loss of the tools in the holes.

The geophysical data acquisition was performed in general accordance with ASTM D5753, Planning and Conducting Boring Geophysical Logging (ASTM, 2010) and ASTM D6274, Conducting Boring Geophysical Logging – Gamma (ASTM, 2004). The geophysical tools included Robertson E-Log, 3-arm mechanical caliper (CAL); and fluid temperature and conductivity (FTC). All three of these tools measure natural gamma (NG). These probes record at up to 0.05-foot sample rate.

A High Resolution Acoustic Televiewer (HIRAT) collected televiewer images at 0.004- foot intervals and borehole deviation data on 0.04-foot intervals. Suspension velocity measurements were performed using the suspension PS logging system. The intervals for downhole geophysical surveys using various methods are summarized in Table 3-3. Appendix G presents the logs of the geophysical surveys.

Table 3-3 Summary of Geophysical Survey Intervals

Core Hole	Date Logged	Caliper	ELOG	FTC	HIRAT	SUSP
		Logging Intervals[1] (feet)				
FS-B1	2/20-22/2016	10-1,001	125-1,000	0-1,001	131-999	131-989
E1-B1	4/14-16/2016 5/1/2016	1-2,700	39-2,700	0-2,697	140-2,700	144- 1,001
E1-B2	4/06-7/2016, 4/12/2016	3-975	36-995	0-979	108-995	123-966
ALT-B2	6/8/2016, 6/11-13/2016	0-1,554	41-1,517	----	54-503, 635-776, 853-1,043, 1075-1,505	----
ALT-B3	8/25-26/2016 9/10-11/2016	0-2,099	30-2,092	0-2,093	30-2,099	41-558

[1] Logging intervals reported are core depths, not vertical depths, and do not include corrections for core hole plunge.

3.4.1 Well Logging

Well logging tools included caliper (CAL), natural gamma, and a Robertson E-Logging system that measures fluid temperature and conductivity (FTC), E-Log [single point resistance, short normal and long normal resistivity (SPR)], natural gamma, and self spontaneous potential (SP).

Caliper and natural gamma data were collected using a mechanical 3-arm caliper probe (CAL). The probe is 6.82 feet long, and 1.5 inches in diameter. As configured, the probe can measure boring diameters between 1.6 and 12 inches.

This probe is useful in the following studies:

- Measurement of boring diameter and volume;
- Location of hard and soft formations;
- Location of fissures, caving, pinching and casing damage;
- Bed boundary identification; and
- Strata correlation between borings.

The caliper consists of three arms, each with a toothed quadrant at their base, pivoted in the lower probe body. A toothed rack engages with each quadrant, constraining the arms to move together. Linear movement of the rack is coupled to opening and closing of the arms. Springs hold the arms open in the operating position. A motor drive retracts the arms, allowing the probe to be lowered into the boring. The rack is coupled to a potentiometer, which converts movement into a voltage sensed by the probe's microprocessor.

Natural gamma measurements rely on small quantities of radioactive material contained in soil and rocks to emit gamma radiation as they decay. Trace amounts of uranium and thorium are present in a few minerals. Feldspar, mica and clays include traces of a radioactive isotope of potassium. The radiation is detected by scintillation - the production of a tiny flash of light when gamma rays strike a crystal of sodium iodide. The light is converted into an electrical pulse by a photomultiplier tube.

The measurement is useful because the radioactive elements are concentrated in certain soil and rock types, e.g., clay or shale, and depleted in others, e.g., sandstone or coal.

Fluid temperature, fluid conductivity and natural gamma data were collected using a temperature/conductivity probe (FTC). The probe is 7.4 feet long and 1.5 inches in diameter.

This probe is useful in the following studies:

- Bed boundary identification;
- Strata correlation between borings;
- Strata geometry and type (shale indication);
- Salt water intrusion; and
- Ground water flow between aquifers.

The temperature probe and conductivity electrodes are located in an insulated cavity at the bottom of probe body, with a fluid inlet opening at the tip and exit openings on the side of the probe approximately 100 millimeters above the tip. This tool is designed to collect data as it is lowered into the boring, so that the boring fluid moves through the cavity and passes over the sensors with a minimum of mixing or disturbance of the fluid by the passage of the probe. For the same reason, this is generally the first probe deployed in a suite of boring geophysical measurements.

E-Log and natural gamma data were collected using an electric log probe (ELOG). This probe measures single point resistance (SPR), short normal (16 inch) resistivity, long normal (64 inch) resistivity, Spontaneous Potential (SP) and natural gamma. The ELGX probe is 8.20 feet long, and 1.73 inches in diameter. The addition of an insulated bridle cable makes the functional length of the tool 41 feet.

This probe is useful in the following studies:

- Bed boundary identification;
- Strata correlation between borings;
- Strata geometry and type (shale indication); and
- Voltages are measured between the 16-inch and 64-inch electrodes and the remote earth connection at surface, as noted below:

Single Point Resistance (SPR): The current flowing to the cable armor is measured along with the voltage at the SPR electrode. The voltage divided by current gives resistance.

Spontaneous Potential (SP): This is the DC bias of the 16-inch electrode with respect to the voltage return at the surface (ground stake).

3.4.2 P-S Suspension

Downhole suspension seismic velocity surveys were performed. The surveys were performed using an OYO suspension P-S logging system to collect velocity data at 3.3-foot intervals in the borings using a 22-foot long probe. Similar to the Acoustic Televiewer (ATV), the suspension probe requires being submerged during operation. The seismic velocity survey measures the compressive (V_p) and shear wave (V_s) velocity of geomaterials adjacent to the probe in the vertical direction. The velocity profiles are plotted for comparison with other rock mass properties in Figure 3-1 through Figure 3-16 (Appendix B).

3.4.3 Acoustic Televiewer

High-resolution acoustic televiewer (HIRAT) logging was performed to create near-continuous oriented images of the boreholes. The HIRAT image is generated from acoustic reflections off the borehole wall and includes a magnetometer and accelerometers to measure the orientation of the probe during data acquisition. The HIRAT sonde must be submerged in water during operation. The sonde detects density contrast in the formation, which are caused by rock discontinuities, bedding planes, clay seams, lithologic changes, etc. The orientations of rock discontinuities that intersect the borehole are reduced from the HIRAT survey and shown on the HIRAT logs in Appendix G.

Boring acoustic images of the boring walls and deviation data of the borings were collected using HIRAT). The probe is 5.32 feet long and 1.65 inches in diameter. In this application, this probe is useful in the following studies:

- Measurement of boring inclination and deviation from vertical;
- Determination of need to correct soil and geophysical log depths to true vertical depths;
- Acoustic imaging of the boring wall to identify fractures, dikes, and weathered zones, and determine dip and azimuth of these features.

3.5 In-Situ Testing

In-situ testing was performed to establish the hydraulic conductivity and groutability of the fractured rock mass, to collect groundwater samples at select intervals, and to estimate the in-situ stress. Appendix H presents additional details about the in-situ testing.

3.5.1 Packer Permeability

In-situ groutability and hydraulic conductivity (packer) testing was performed in each of the rock core borings using inflatable packers. The packer system can be configured as a single or dual (straddle) assembly to isolate selected sections of formation for testing and includes a transducer housing in the test interval to measure in-situ testing pressures. Geotechnical professionals oversaw testing and collected test data in accordance with the methods and procedures described in the Engineering Geology Field Manual (USBR, 1998). Table 3-4 summarizes the number and type of packer tests performed at each rock core boring. Appendix H presents information regarding the testing and the individual test results. The packer test results are presented for comparison with other rock mass properties in Figure 3-1 through Figure 3-16 (Appendix B). Test intervals with no measurable volume of water injected are assumed to have rock mass hydraulic conductivities between 10^{-8} and 10^{-7} centimeters per second (cm/sec).

Table 3-4 Summary of Packer Permeability (Lugeon) Testing

Core Hole	No. of Tests	Single-Packer	Dual-Packer
FS-B1	15	11	4
E1-B1	7	4	3
E1-B2	8	5	3
ALT-B2	13	10	3
ALT-B3	5	0	5

3.5.2 Groundwater Sampling

The main purposes of groundwater sampling were to evaluate groundwater residence time (i.e., date the groundwater age), evaluate the isotopic signature of the groundwater with depth, and understand the general chemistry of groundwater at the Study Area with an overall objective of evaluating the potential impact of tunneling on groundwater and surface water resources in the investigation area. The initial objectives included the following:

1. Characterize the natural groundwater chemistry within the region of the proposed tunnel.
    a) Identify varying chemistry within different rock types.
    b) Identify varying chemistry within fault zones.
2. Test groundwater chemistry at different depths to evaluate hydrogeology at and above the proposed tunnel and to evaluate the potential for system losses due to groundwater discharge to the tunnel.
    a) Characterize vertical hydraulic connectivity within the aquifer system.
3. Evaluate whether fault zones are potential groundwater conduits and/or barriers.
4. Collect isotope chemistry from the groundwater to assess groundwater age.

Groundwater samples were collected from Core Holes FS-B1, E1-B1, ALT-B2, and ALT B3. Samples could not be collected from Core Hole E1-B2 due to unstable borehole conditions. Groundwater sample depths were selected based on review of rock core and logged geologic structure, drilling behavior (e.g., circulation loss), downhole geophysics, and other available information. Groundwater samples were collected from identified discrete fractures or fracture zones identified during rock core drilling and logging, and acoustic televiewer results. Quality-control (QC) samples were collected to evaluate the potential impact of drilling fluid on groundwater samples. These included a source-water blank from the pool near Core Hole FS-B1 and two drilling-fluid blanks sampled from the mud used at Core Holes FS-B1 and E1-B1. The QC samples, sampling depth intervals, lithology, and the reason for selecting each sampling depth in project core holes are provided in Table 3-5.

Table 3-5 Summary of Groundwater Sampling Intervals

Core Hole	Sample ID	Date	Top of Sample Interval (core depth in feet)	Bottom of Sample Interval (core depth in feet)	Length of Sample Interval (feet)	Lithology	Reason Targeted
FS-B1	FSB1-DF (Drilling Fluid)	2/16/2016	NA	NA	NA	NA	NA
FS-B1	E1B1-DF (Drilling Fluid)	2/16/2016	NA	NA	NA	NA	NA
Source Water	FSB1-SB (Source Water)	2/16/2016	NA	NA	NA	NA	NA
FS-B1	FSB1-GW-140-200	3/4/2016	140	200	60	syenite/ gabbro	First encountered groundwater
FS-B1	FSB1-GW-191-201	2/15/2016	191	201	10	syenite/ gabbro	First encountered groundwater
FS-B1	FSB1-GW-386-396	2/24/2016	386	396	10	anorthosite w/gabbro	Potentially fault zone, fracture patterns observed during drilling
FS-B1	FSB1-GW-937-947	2/23/2016	937	947	10	gabbro/ anorthosite	Change of lithology/fault, fracture patterns observed during drilling
E1-B1	E1-B1-GW-2380-2390	4/21/2016	2380	2390	10	anorthosite/ gabbro	Deep water, fracture patterns observed during drilling
E1-B2	E1-B2	Samples were not collected due to unstable corehole conditions					
ALT-B2	ALT-B2-GW-120-168	5/1/2016	120	168	48	granite/ granodiorite	First encountered groundwater
ALT-B3	ALT-B3-GW-112-223	5/15/2016	112	223	111	granite/ granodiorite	First encountered groundwater

Core Hole	Sample ID	Date	Top of Sample Interval (core depth in feet)	Bottom of Sample Interval (core depth in feet)	Length of Sample Interval (feet)	Lithology	Reason Targeted
ALT-B3	ALT-B3-GW-2015-2035 (day 1)	8/30/2016	2015	2035	20	granite/ granodiorite	Deep water, fracture patterns observed during drilling
ALT-B3	ALT-B3-GW-2015-2035 (day 2)	8/31/2016	2015	2035	20	granite/ granodiorite	Deep water, fracture patterns observed during drilling
ALT-B3	ALT-B3-GW-2015-2035 (day 3)	9/1/2016	2015	2035	20	granite/ granodiorite	Deep water, fracture patterns observed during drilling

NA = Not Applicable

In addition to measurement of several field parameters during purging and sampling, groundwater and QC samples were analyzed for major ions, metals, and selected radionuclides to characterize general chemistry and patterns of water quality. Samples were analyzed for a suite of environmental tracers that included the stable isotopes of oxygen, hydrogen, and carbon, and radioactive isotopes of carbon (^{14}C) and hydrogen (tritium, ^{3}H). These environmental tracers were used to investigate sources of recharge, groundwater ages, and travel times, and to support the development of a conceptual model of the groundwater flow system. The sampling methodology is described in Appendix J.

3.5.2.1 Sampling Depths and Conditions

Core Hole FS-B1

Sampling depth intervals 140-200, 191-200, 386-396, and 937-947 feet bgs were selected based on fracture patterns observed during core logging and geophysical imaging. Purging and sampling procedures in corehole FS-B1 at depth intervals 191-200, 386-396, and 937-947 feet were conducted with the pneumatic system. The depth interval between 140-200 feet was purged using the Grundfos pump.

Core Hole E1-B1

The sampling depth interval 2380-2390 feet bgs was selected based on fractures observed during corehole logging and geophysical imaging. Only one depth interval was chosen for this hole due to predominantly unfractured borehole conditions. Two samples were collected from this interval to evaluate temporal changes in chemistry during purging. However, the recharge rate decreased during purging resulting in a reduced analyte list for the second sample due to time constraints. Purging and sampling were performed using the Panacea pump.

Core Hole E1-B2

Water samples were not collected from Core Hole E1-B2 due to unstable conditions.

Core Hole ALT-B2

The sampling depth interval 120-168 feet bgs was selected based on anticipated groundwater levels from regional data. The deep interval, 2015-2035 feet bgs, was selected based on fractures observed during core hole logging and geophysical imaging. Purging and sampling of depth interval 120-168 feet bgs was achieved with the Grundfos pump. The deeper interval was purged and sampled using the pneumatic pump.

Core Hole ALT-B3

The sampling depth interval 112-223 feet bgs was selected to sample first-encountered groundwater. The sampling depth interval 2015-2035 feet bgs was selected based on fractures observed during core logging and geophysical imaging. Three samples (one per day) were collected during purging of the deep interval to evaluate temporal changes in chemistry during purging. Purging and sampling of the shallow depth interval was achieved with the Grundfos pump, while purging and sampling the deep depth interval was achieved using the pneumatic pump.

GAMA Program

In addition to samples from the four core holes, analytical data for four wells within the Study Area boundaries sampled as part of the United States Geological Survey (USGS) Groundwater Ambient Monitoring (GAMA) program (Davis and Shelton, 2014) are included in Table I-8 and laboratory-results summary tables (Sections 5.6 and 5.7) for comparison. These wells were sampled in 2011 and include GAMA-SG-03 (production well), GAMA-SG-08 (production well), GAMA-SG-21 (spring well), and GAMA-SG-24 (production well). The screen intervals for these wells are unknown; only well GAMA-SG-08 has a known total well depth of 800 feet bgs.

3.5.3 In-Situ Stress Determination

In-situ stress testing was performed in accordance with ASTM D4645 to determine the state of stress in the rock mass in Core Holes E1-B1 and ALT-B3. This test method utilizes a high-pressure straddle packer system to isolate an intact zone within a vertical rock core boring and hydraulically fracture the rock core boring within the test zone. HIRAT imaging was performed in the interval both before and after in-situ testing to help identify suitable test intervals and observe the resulting test features and orientations. Table 3-6 summarizes the in-situ stress determination test intervals and results. Appendix H presents information on the testing and the individual test results. The results are discussed in Section 5.

Table 3-6 Summary of In-Situ Stress Determination Testing

Core Hole	Test No.	Rock Unit	Lithology	Test Interval[1]		Breakdown Pressure	Re-frac Pressure	Shut-in Pressure	Max. Horiz. Stress (σ_H)	Trend of Max. Horiz. Stress	Min. Horiz. Stress (σ_h)	Trend of Min. Horiz. Stress
				feet		psi	psi	psi	psi	degrees	psi	degrees
E1-B1	1	Anorthosite	anorthosite	1,850.0	1,853.3	2096	1870	1460	1554	140-320	1460	50-230
E1-B1	2	Anorthosite	anorthosite	1,858.0	1,861.3	2190	1640	1410	1700	140-320	1410	50-230
E1-B1	3	Anorthosite	anorthosite	2,035.0	2,038.3	1701	1470	1360	1905	158-338	1360	68-248
E1-B1	4	Anorthosite	anorthosite	2,039.0	2,042.3	1789	1630	1380	1607	158-338	1380	68-248
E1-B1	5	Anorthosite	anorthosite	2,155.0	2,158.3	2300	1820	1550	1725	111-291	1550	21-201
E1-B1	6	Anorthosite	anorthosite	2,159.0	2,162.3	2689	1640	1410	2136	111-291	1720	21-201
E1-B1	7	Anorthosite	anorthosite and granite	2,324.7	2,328.0	2590	1740	1480	1537	061-241	1480	151-331
E1-B1	8	Anorthosite	anorthosite and granite	2,328.7	2,332.0	2549	1820	1560	1680	061-241	1560	151-331
ALT-B3	1	Granite	granite	2,063.5	2,066.8	3235	2510	2350	3012	144-324	2350	54-234
ALT-B3	2	Granite	granite	2,069.5	2,072.8	3182	2600	2320	2929	144-324	2320	54-234
ALT-B3	3	Granite	granite	2,074.0	2,077.3	4485	2790	2460	3372	137-317	2460	47-227
ALT-B3	4	Granite	granite	2,079.5	2,082.8	5865	2280	2040	2857	137-317	2040	47-227

[1] Test intervals reported are core depths not vertical depths, and do not include corrections for core hole plunge.

4 LABORATORY TESTING

Laboratory testing program included soil, rock, and groundwater testing methods. Test results and summaries are included in Appendix I.

4.1 Soil Testing

The ANF geotechnical investigation did not include drilling methods to obtain relatively undisturbed samples of surficial soil or unconsolidated sediments (fill, colluvium, and landslide mass). However, we selected soil test methods (Table 4-1) to classify granular and fine-grained soil-like materials infilling rock discontinuities and other intermediate geomaterials (e.g., fault breccia, gouge, cataclasite, and weathered or very soft rock types) and to estimate their engineering properties. Intervals of testing on samples are noted on the rock core boring logs (Appendix D).

Table 4-1 Summary of Soil Testing Methods

Test Method (Abbreviation)	Test Method Designation (Method)	Purpose	No. of Tests Completed
Particle Size Analysis (PA)	ASTM D422 & D1140	Establish particle size gradations	7
Atterberg Limits (PI)	ASTM D4318	Establish Atterberg Limits and plasticity of fine-grained materials	7
Swell Potential (SP)	ASTM D4546	Establish swell pressure of clay-rich materials	1

Source: ASTM, 2016

4.2 Rock Testing

Rock mechanics and tunnel boring machine (TBM) related laboratory testing methods are highly specialized and are performed primarily for classification and index testing, or to help establish engineering properties of the rock mass (characterization). The rock laboratory testing methods are summarized in Table 4-2.

Table 4-2 Summary of Rock Testing Methods

Test Method (Abbreviation)	Test Method Designation	Purpose	No. of Tests Completed
Unconfined Compression (UC)	ASTM D7012	Estimate intact rock strength and elastic moduli	48
Confined Compression (CC)	ASTM D7012	Estimate rock strength and elastic moduli	15
Direct Shear (DS)	ASTM D5607	Estimate shear strength of natural joint planes	17
Brazilian Tension (BT)	ASTM D3977	Estimate intact rock tensile strength	13
Point Load (PL)	ASTM D5731	Index of intact rock strength	79

Test Method (Abbreviation)	Test Method Designation	Purpose	No. of Tests Completed
Slake Durability (SLK)	ASTM D4644	Index of susceptibility to slaking	6
Punch Penetration (PUN)	Non-ASTM	TBM cutterhead design	7
Cerchar Abrasion (CAI)	ASTM D7625	Index of rock abrasivity	7
Petrographic Analysis (PET)	Non-ASTM	Classify mineralogy and abrasivity using optical methods	29
X-ray Diffraction (XRD)	Non-ASTM	Classify clay mineralogy using X-ray powder diffraction methods	9

Source: ASTM, 2016

4.3 Groundwater Testing

Table 4-3 lists the analytes for groundwater samples. Groundwater samples were analyzed using the methods described in Appendix J.

Table 4-3 Summary of Groundwater Testing Methods

Analyte Groups	Analyte
General Chemistry[1]	total hardness, calcium, magnesium, sodium, potassium, total alkalinity, hydroxide, carbonate, bicarbonate, chloride, sulfate, nitrate as nitrogen (N), fluoride, total dissolved solids (TDS), and nitrite as N
Dissolved Metals[1]	mercury, antimony, arsenic, barium, beryllium, cadmium, total chromium, cobalt, copper, lead, manganese, molybdenum, nickel, selenium, silver, thallium, vanadium, and zinc
Radionuclides[2]	gross alpha, gross beta, radium-226, radium-228, strontium-90, and uranium
Stable Isotopes and Carbon-14 (^{14}C)[3]	oxygen-18 ($\delta^{18}O$), deuterium (δD), and carbon-13 ($\delta^{13}C$)
Tritium in Water[4]	Tritium (^{3}H)[4]

[1] Babcock Laboratories, Riverside, California
[2] FGL Environmental Agricultural Analytical Chemists, Santa Paula, California
[3] Beta Analytic, Inc., Miami, Florida
[4] University of Miami, Rosenstiel School of Marine and Atmospheric Science, Miami, Florida

The groundwater samples had sufficient carbon and hydrogen for accurate radiocarbon and deuterium measurements, respectively, and to validate laboratory results. In addition, the analytical results of general chemistry, metals, and radionuclides were validated for precision and accuracy by the respective laboratories. Quality control and quality assurance were completed by the laboratories and detailed discussions are included in Appendix J. The ^{14}C results were obtained from dissolved inorganic carbon (DIC) and are reported both as percent modern carbon (pMC) and fraction modern carbon ($F^{14}C$). Tritium concentrations are expressed in tritium units (TU), where 1 TU indicates a T/H abundance ratio of 10^{18}. The values refer to the tritium scale recommended by US National Institute of Science and Technology (NIST, formerly NBS), and International Atomic Energy Agency (IAEA), and results were validated by the laboratory. The laboratory reports include the method used, material type, and applied pretreatments (Appendix J).

5 RESULTS

The results and data presented here are to assist in the feasibility evaluation of the proposed tunnels under the ANF. These results are applicable at the rock core boring locations and some of the information may vary because of seasonal fluctuations (e.g., groundwater pressures, ambient temperatures, etc). The extrapolation or use as analogs to other locations within the ANF may or may not be representative and these judgements should be made only by qualified licensed geo-professionals. Figures referenced in this section are included in Appendix B.

5.1 Subsurface Conditions at Rock Core Borings

The subsurface conditions encountered in each of the core holes are presented below and summarized on Figure 3-1 through Figure 3-16 (Appendix B).

Core Hole FS-B1 was selected to characterize the rock conditions of the syenite and anorthosite complex, and the Transmission Line fault zone separating them. At Core Hole FS-B1, the predominant lithologies from the ground surface to about 355 feet are syenite and gabbro. Fault breccia comprising the Transmission Line fault zone occurred at approximate core depths of 355 to 360 feet. However, evidence of shearing is not localized explicitly to this zone. From approximate core depths 360 to 1,004.7 feet, the predominant lithology is anorthosite with lesser apophysis, inclusions, or dikes of gabbro.

Core Hole E1-B1 was selected to characterize the anorthosite complex. At Core Hole E1-B1, the predominant lithologies from the ground surface to about 124 feet are leucogabbro and gabbro. Below 124 feet, the predominant lithologies are anorthosite and gabbro with lesser dikes of granite and pegmatite (very coarse- to coarse-grained granite).

Core Hole E1-B2 was selected to characterize the rock conditions of the granite and granodiorite, and part of the San Gabriel Fault Zone. At Core Hole E1-B2, fill, colluvium and debris flow deposits overly bedrock. Fill was inferred from the ground surface to depth of 20.5 feet and comprised of mixtures of silt, sand and gravel. Colluvium and debris flow deposits were encountered from depths of 20.5 to 89.7 feet and were comprised of materials recovered as gravel, cobbles, silt and sand. From core depths of 89.7 to 1,005.9 feet, the predominant lithologies are granite and granodiorite. The faulting and resulting mechanical and chemical weathering of the granite and granodiorite varies and several brecciated zones and zones with gouge occur throughout this rock core boring. Fault gouge comprising a fault presumably related to the San Gabriel Fault Zone occurs from approximate core depths of 657 to 674 feet.

Core Hole ALT-B2 was selected to characterize San Gabriel fault and the adjacent rock conditions resulting from this structure. The predominant lithologies at this rock core boring location include gneiss, fault breccia, and flaser granodiorite. From the ground surface to core depth of 1,029 feet, gneiss is the predominant lithology and ranges from relatively intact gneiss, to brecciated gneiss and gouge. There are two concentrated zones of fault breccia and gouge interpreted as faults of the San Gabriel fault zone, from approximate core depths of 1,029 to 1,065 feet and 1,532 to 1,563 feet. During drilling operations, core hole instabilities and obstructions coinciding with these zones were experienced. From inspection of the core samples and laboratory testing, the gouge from these zones is classifiable as a Sandy Lean CLAY (CL) to Clayey SAND (SC) using the Unified Soils Classification System. From approximately 1,065 to 1,532 feet and from 1,563 to 1,618 feet, flaser granodiorite is the predominant lithology. The descriptor, “flaser”, is used to describe a lithology comprised of relatively unaltered lenses, layers or blocks of rock bounded by zones of sheared/crushed material.

Core Hole ALT-B3 was selected to characterize the rock conditions within the granodiorite south of the San Gabriel fault. From ground surface to approximate core depth of 1,734 feet, granodiorite and dikes of granite, mylonite, and gabbro are the predominant lithology. A sheared and altered zone within the granodiorite occurs from approximately 1,365 to 1,385 feet. From approximately 1,734 to 2,100 feet, granite is the predominant lithology.

5.2 In-Situ Groundwater Pressures

In-situ groundwater pressures were measured using VWP installed within the rock core borings. Figure 5-1 through Figure 5-5, present profiles of the in-situ groundwater pressures with depth at the rock core boring locations. Hydrostatic trends [i.e., a pressure gradient corresponding to the unit weight of water 0.433 pounds per square inch (psi) per foot] are assumed and plotted to show instruments potentially collecting readings from a single connected fractured rock mass aquifer. At locations where there appears to be multiple fractured rock mass aquifers, the boundaries where shown on Figure 5-2, Figure 5-5, Figure 5-8, Figure 5-11 and Figure 5-14 (Appendix B) are roughly interpreted using other observed rock mass conditions or taken arbitrarily as the average vertical distance between successive VWPT defining different aquifers.

At Core Hole FS-B1 (Figure 5-1 through Figure 5-3) the four vibrating wire pressure transducers (VWPT) have groundwater pressures that can be connected assuming a single hydrostatic trend. This trend is indicative that locally at Core Hole FS-B1, there is a single fractured rock mass aquifer that can be considered analogous to a porous aquifer when estimating groundwater pressures. Based on the readings taken on August 10, 2016, the shallowest VWPT (VWPT-1) indicates the depth to water from ground surface is approximately 131 feet. Assuming a hydrostatic pressure gradient [0.433 pounds per square inch (psi) per foot] starting at a depth bgs of 131 feet and projecting downward correcting for rock core boring plunge approximates the groundwater pressure measured by the VWPT successively installed at deeper intervals.

At Core Hole E1-B1 (Figure 5-4 through Figure 5-6), the five VWPT cannot be all connected using a single hydrostatic trend indicating multiple fractured rock mass aquifers. Groundwater conditions at this location should not be considered as analogous to a porous aquifer when estimating groundwater pressures, but rather the VWPTs can be grouped in four hydraulic trends considering up to four different fractured rock mass aquifers, each with a unique potentiometric surface defined using:

- VWPT-1, for the shallowest aquifer;
- VWPT-2 and VWPT-3;
- VWPT-4; and
- VWPT-5, for the fourth, deepest aquifer.

The groundwater pressure trends at Core Hole E1-B2 indicate potentially two fractured rock mass aquifers locally (Figure 5-8) defined using:

- VWPT-1, for the shallowest aquifer, and
- VWPT-2, VWPT-3, and VWPT-4 for the deepest aquifer.

The groundwater pressure trends at Core Hole ALT-B2 indicate potentially three fractured rock mass aquifers locally (Figure 5-11) defined using:

- VWPT-1, for the shallowest aquifer;
- VWPT-2 and VWPT-3; and
- VWPT-4 and VWPT-5 for the deepest aquifer.

The groundwater pressure trends at Core Hole ALT-B3 indicate potentially three fractured rock mass aquifers locally (Figure 5-14) defined using:

- VWPT-1, for the shallowest aquifer;
- VWPT-2 and VWPT-3; and
- VWPT-4 and VWPT-5 for the third aquifer.

5.3 In-Situ Ground Temperatures

In-situ ground temperatures are measured using the VWPT installed within the rock core borings. Figure 5-16 (Appendix B) depicts a profile of the in-situ ground temperatures measured from the VWP at each rock core boring location. Geothermal gradients differ by location, but at each location the site-specific geothermal gradient does not differ substantially with depth. Therefore, linear equations approximating the geothermal gradient at each location are summarized in Table 5-1. Upon inspection of Figure 5-16, the geothermal gradients are bounded by the linear trends established from Core Holes E1-B2 (upper bound) and E1-B1 (lower bound). The variation in the geothermal gradients are likely due to variations in lithology, hydrogeology, regional tectonics and faulting.

Table 5-1 Summary of Linearized Geothermal Gradients

Core Hole	Geothermal Gradient[1] (degrees Centigrade per foot)	Temperature Intercept[1] (degrees Centigrade)
FS-B1	+0.0082	12.3
E1-B1	+0.0051	12.1
E1-B2	+0.0070	17.2
ALT-B2	+0.0059	14.3
ALT-B3	+0.0051	12.8

[1] Temperatures can be reliably estimated using the constants above in equations of the form $y = mx+b$: Temperature (Depth) = Geothermal Gradient x Depth + Temperature Intercept

5.4 Geophysical Results

The geophysical tooling and methods are described in Section 3.4 and Appendix G. The results of the geophysical surveys are used in conjunction with the rock core logs to assess the subsurface conditions described in Subsection 3.2.1 and aid in development of the rock mass characterization discussed in Section 5.9.

5.5 Hydraulic Conductivities (Lugeon Values)

Rock mass permeability in crystalline (igneous and metamorphic) and moderately-cemented rocks is typically governed by secondary porosity (i.e., by discontinuity conditions). However, each test interval comprises a single, discrete, representative elementary volume, which includes the combined hydrogeologic properties of the intact rock and discontinuities (i.e., primary and secondary porosity, respectively).

In tunneling applications, rock mass hydraulic conductivities are reported in units of Lugeon. A Lugeon is the water loss of 1 litre per minute per meter length of test section at an effective pressure of 1 MegaPascal (MPa). A Lugeon is approximately equivalent to 1x(10^{-5}) centimeters per second (cm/sec). Table 5-2 provides a generalized convention for describing rock mass permeability using Lugeon values.

Table 5-2 Lugeon Values and Rock Mass Permeability Descriptors

Lugeon	Hydraulic Conductivity (K)	Permeability	Rock Mass Conditions
	cm/sec		
<1	< 1x10^{-5}	Low	Tight joints
1-5	1x10^{-5} – 5x10^{-5}	Low to Moderate	Small joint openings
5-50	5x10^{-5} to 5x10^{-4}	Moderate to High	Some open joints
>50	>5x10^{-4}	High	Many open joints

Source: Fell et al., 2005

Figure 5-17 (Appendix B) presents the packer test results as a histogram using the descriptors in Table 5-2. The Lugeon values range from 0.0 (Core Hole E1-B1 core depth 551.9 to 577.9 feet) to 8.05 (Core Hole ALT-B3 925.0 to 935.0 feet) and are indicative of low to moderate rock mass permeabilities, respectively.

5.6 Groundwater Chemistry

Results for field parameters (DO, EC, pH, ORP, temperature, and turbidity) and laboratory analysis of general chemistry, metals, radionuclides, and alkalinity and associated parameters (bicarbonate and carbonate concentrations) are presented in Table J-2. Discussion of measured values is presented in the following sections.

5.6.1 Analytical Testing Results

Field parameter values and groundwater sample laboratory analytical results from the four coreholes and the USGS GAMA program wells are provided below. The results of field parameter measurements and groundwater samples collected from the Study Area were compared to groundwater samples collected and field parameters measured for the USGS GAMA program wells (**Error! Reference source not found.**).

5.6.1.1 Field Parameters

Field parameters measured during the Study Area groundwater sampling and investigation (field parameters were not measured in QC samples) are summarized in the following:

- DO – results from the four core holes ranged from 0.25 milligram per liter (mg/L) (FSB1-GW-140-200) to 7.29 mg/L (ALT-B3-GW-2015-2035_1). The DO values from the USGS GAMA program ranged from 1.5 to 6.4 mg/L, which are comparable and within the range of values measured during the current investigation.
- EC – ranged from 0.589 (ALT-B3-GW-112-223) milliSiemens per centimeter (mS/cm) to 1.78 mS/cm (ALT-B3-GW-2015-2035_3). The EC values from the USGS GAMA program are 0.454 to 0.830 mS/cm and are comparable and within the range of values measured during the current investigation.
- pH – results from the four core holes ranged from 7.21 (ALT-B3-GW-2015-2035_3) to 8.38 (FSB1-GW-191-201), and USGS GAMA program values ranged from 6.8 to 7.4. The pH values are comparable.
- ORP – results from the four core holes range from -228 (FSB1-GW-386-396) millivolts (mV) to 18 mV (ALT-B3-GW-2015-2035_1). ORP data are not reported for the USGS GAMA samples.
- Temperature – results from the four coreholes ranged from 13.37 (ALT-B3-GW-112-223) degree Celsius (°C) to 29.74 °C (ALT-B3-GW-2015-2035_1). The temperatures from the USGS GAMA program (11.5 to 19 °C) are comparable.
- Turbidity – results from the four core holes ranged from 27 (ALT-B3-GW-2015-2035_3) Nephelometric Turbidity Units (NTU) to 685 NTU (FSB1-GW-386-396). Turbidity data are not reported for the USGS GAMA samples.
- Ferrous iron and sulfide – ferrous iron was only detected in FSB1-GW-140-200 at 0.5 mg/L and FSB1-GW-937-947 at 2.5 mg/L. Sulfide was not detected in any samples. Ferrous iron and sulfide are not reported for the USGS GAMA samples.

5.6.1.2 General Chemistry

Water-quality data collected during this investigation and data collected by the USGS GAMA program are included in Table J-1. Cation and anion data were evaluated first with regards to electric neutrality. Because water samples do not contain an electrical charge, the sum of all positively charged ions (cations), primarily sodium, potassium, calcium, and magnesium should equal the sum of all negatively charged ions (anions), primarily chloride, bicarbonate, sulfate, and nitrate. Concentrations were converted to milliequivalents per liter (meq/L) and a cation/anion balance was computed using:

$$\text{Cation/Anion Balance} = [(\Sigma \text{ cations} - \Sigma \text{ anions}) / (\Sigma \text{ cations} + \Sigma \text{ anions})] * 100$$

If all laboratory analyses are done perfectly, the ideal analysis should have a cation/anion balance of zero percent. Positive balances indicate the sum of cations is greater than the sum of anions; negative balances indicate that the sum of anions is greater than the sum of cations. The samples had cation/anion balances within ±10 percent.

The results of the general chemistry for QC and groundwater samples are summarized in the following:

- Major Cations – sample results for calcium, magnesium, potassium, and sodium are comparable to values from the USGS GAMA program.
- Major Anions – sample results for chloride, bicarbonate, and sulfate are comparable to values from the USGS GAMA program.
- Total alkalinity – sample results ranged from 85 mg/L (ALT-B3-GW-2015-2035_3) to 590 mg/L (FSB1-DF), and results for the USGS GAMA program were 165 to 333 mg/L.
- Total Dissolved Solids – sample results ranged from 350 mg/L (E1-B1-GW-2380-2390) to 2800 mg/L (FSB1-DF), and results for the USGS GAMA program were 295 to 515 mg/L.
- Nitrate as N and Nitrite as N – sample results ranged from not detected to 1.4 mg/L, and results for the USGS GAMA program were not detected to 0.47 mg/L.
- Total Hardness – sample results ranged from 150 microgram per liter (µg/L) (E1-B1-DF) to 830 µg/L (ALT-B3-GW-2015-2035_3). Total hardness data are not reported for the USGS GAMA program.

Metals

The analytical results for metals are summarized in the following:

- Arsenic, barium, copper, manganese, mercury, molybdenum, nickel, chromium, and zinc were detected in the QC samples and groundwater samples collected from the four core holes. Mercury was not analyzed, but antimony, beryllium, cadmium, lead, selenium, and vanadium were detected in in USGS GAMA program groundwater samples.

Radionuclides

Radionuclides results from the Study Area groundwater sampling and investigation are summarized in the following:

- Gross Alpha – the gross alpha activity was less than 8 picocurie per liter (pCi/L) in samples from the four core holes and blanks. The highest detected value was 7.98 pCi/L (E1-B1-GW-2380-2390). The results of gross alpha values are comparable to the results for the USGS GAMA program, although the average value for GAMA samples is lower.
- Gross Beta – the gross beta activity was less than 10 pCi/L in samples from the four core holes and blanks. The highest reported value was 9.86 pCi/L (ALT-B3-GW-2015-2035_3). The results of gross beta values are comparable to the results reported for the USGS GAMA program, although the average value for GAMA samples is lower.
- Radium, Strontium, and Uranium – these radionuclides were not detected or were detected at low concentrations in samples from the four core holes and blanks. Radium, strontium, and uranium data were not reported for the USGS GAMA samples.

$\delta^{13}C$, $\delta^{18}O$, AND δD

Depending upon its source and travel history, the groundwater in the Study Area has a particular $^{13}C/^{12}C$ ratio, which is reported using the standard delta (δ) notation in units of parts per thousand (‰ or per mil).

$$\delta^{13}C = (R_{sample}/R_{standard} - 1) \times 1000$$

where, R_{sample} and $R_{standard}$ represent $^{13}C/^{12}C$ ratios of the sample and the international standard (VPDB), respectively. Similarly, $^{18}O/^{16}O$ and $D/^{1}H$ ratios can be used in the above equation for oxygen $\delta^{18}O$ and deuterium δD relative to the SMOW international standard. Physical mixing and chemical reactions produce changes in the isotopic composition of the water.

Measurement of stable hydrogen and oxygen isotopes in water can be a useful tool to examine the recharge history of groundwater, because hydrogen and oxygen are part of the water molecule and generally are not affected by processes that may affect dissolved constituents (Kendall and McDonnell, 1998). Groundwater and QC sample results for $\delta^{13}C$, $\delta^{18}O$, and δD are presented in Table J-3 with average values of -14.2‰, -7.7‰, and -56.4‰, respectively. The results for the USGS GAMA program are comparable, but slightly lighter isotopically, to the results for this study.

Carbon 14 and Tritium

The combination of the radioactive isotopes of hydrogen (tritium) and carbon (carbon-14) is effective for locating sources of recharge, determining the age (time since recharge) of ground water, and identifying geologic controls on the movement of ground water. Results for carbon-14 and tritium are provided in Table J-3.

In addition to natural sources, carbon-14 was produced by the atmospheric testing of nuclear weapons, and carbon-14 activities may exceed 100 pMC in areas where groundwater contains tritium from nuclear weapons tests. Carbon-14 activities are used to determine the age (time since recharge) of ground water on time scales ranging from recent to more than 20,000 years before present. Because carbon-14 is not part of the water molecule, its activity and interpreted carbon-14 ages may be affected by reactions between constituents dissolved in ground water and aquifer materials.

Carbon-14 activities for water collected from the four core holes, source water, and drilling fluid in the Study Area ranged from 57.0 to 96.2 pMC with an average value of 85.2 pMC. The highest carbon-14 activities, exceeding 90 pMC, were in water from samples taken from FS-B1-SB (Source Water Blank), FS-B1-GW-191-201, FS-B1-GW-140-200, and E1-B1-GW-2380-2390-B (Table J-3). The apparent radiocarbon age estimated for the Study Area groundwater samples ranges from 380 year before present (years BP) to 4,520 years BP. Most of the groundwater samples for the USGS GAMA program for the Study Area exceeded 100 pMC, with a high value of 104 pMC. Even though the age of the water samples is not provided, the carbon-14 data reported by USGS GAMA program suggest younger water than the results for the core hole samples.

Tritium was detected in all of the water samples collected from the Study Area. The highest tritium detected in Study Area samples is 2.82 TU. Tritium activities for water collected from the four coreholes, source water, and drilling fluid at the Study Area ranged from 1.14 to 2.82 TU with an average value of 2.19 TU. The average tritium activity for the USGS GAMA program for the Study Area is 7.63, approximately three to four times higher than the average tritium activity in this study; tritium activities ranged from 5.30 to 9.83 TU.

5.6.2 Analytical Results Discussion

Groundwater geochemistry data were evaluated to assess natural conditions in the Study Area based on both core hole and USGS GAMA results. Cation and anion results for 17 samples including core holes, four wells from the USGS GAMA program, and QC samples were plotted on a trilinear diagram (also known as a Piper diagram) and Stiff Diagrams to examine water types and to assess whether groundwater samples could be distinguished on the basis of depth and/or lithologic unit (Figure 5-18 and Figure 5-19). The potential influence of drilling fluids may be evaluated. A Piper diagram is a trilinear plotting system in which each sample analysis is represented by a single point, permitting large numbers of analyses to be presented on a single diagram (Piper, 1944). Concentrations of chloride, bicarbonate, carbonate, sulfate, sodium, potassium, calcium, and magnesium in mg/L are normalized by conversion to meq/L and then percentages of each are calculated and plotted. The diagram consists of two lower triangular regions, one for cations and one for anions, with a diamond-shaped region above and between the triangles into which points from the triangles are projected. The intersection of these projections represent the composition of the water with respect to the combination of ions shown.

A Stiff diagram permits interpretation of water chemistry by means of distinct graphical shapes. It consists of three horizontal axes extending on each side of a vertical zero axis and displays the same ions as a Piper diagram (also in meq/L) with the four cations (sodium and potassium are added together for one axis) on the left side and the four anions (bicarbonate and carbonate are added together for one axis) on the right (Stiff, 1951). The area of the region is an approximate indication of the total ionic content.

The major ion composition of groundwater collected from the wells, as illustrated by the Piper and Stiff diagrams, is generally dominated by sodium, bicarbonate, and calcium ions. Data reported by the USGS GAMA program for the Study Area were used to evaluate and compare the geochemical types of the groundwater. Figure 5-18 and Figure 5-19 present the groundwater and quality-control sample Piper and Stiff Diagrams, respectively. Results for the QC samples indicate that their anion proportions are similar to most groundwater samples except for the day 2 and day 3 samples from Core Hole ALT-B3 at 2015-2035 ft bgs. Cation results for the QC drilling-fluid samples are generally different than the groundwater samples, again except for the day 2 and day 3 samples from Core Hole ALT-B3 at 2015-2035 ft bgs.

The shallow and deep groundwater at Core Hole FS-B1 and E1-B1 is primarily sodium-bicarbonate ($Na\text{-}HCO_3$) type, whereas the shallow groundwater from core holes ALT-B2, ALT-B3, and groundwater from USGS GAMA program wells are primarily calcium bicarbonate ($Ca\text{-}HCO_3$) type. The deep groundwater from Core Hole ALT-B3 has two distinctive water types, $Ca/Na\text{-}HCO_3$ (day 1) and calcium sulfate ($Ca\text{-}SO_4$) (days 2 and 3), with $Ca\text{-}SO_4$ likely being most representative of deep groundwater conditions due to the additional purging prior to collecting those samples. The general similarity between the chemistry for the current study in 2016 and the USGS GAMA program in 2011 indicates that groundwater conditions remained similar during these two periods. Most of the groundwater samples show similar cation-anion characteristics, indicating a common origin(s) of water. The linear alignment of QC and most groundwater cation results and the general similarity between QC and most groundwater anion results suggests that drilling fluids may have impacted the Study samples. However, results for GAMA groundwater samples indicate that shallow groundwater may be primarily $Ca\text{-}HCO_3$ to $Ca/Na\text{-}HCO_3$ type in the Study Area. As indicated, deep groundwater, at least at the location of Core Hole ALT-B3, appears to be $Ca\text{-}SO_4$ type.

The concentrations of both sodium and bicarbonate are prominent in Study Area samples. However, while this can be due to the dominance of silicate weathering in the crystalline basement rock, it may be caused by residual impact from drilling fluids. While about 50 percent of the groundwater samples plot within the field of sodium – bicarbonate ($Na\text{-}HCO_3$) type, this is similar to the drilling-fluid samples, and shallow groundwater not impacted by drilling fluid is most likely $Ca\text{-}HCO_3$ type.

Dissolved carbon dioxide, bicarbonate, and carbonate are the principal sources of alkalinity, or the capacity of solutes in water to neutralize acid. Carbonate contributors to alkalinity include atmospheric and biologically-produced carbon dioxide, carbonate minerals, and biologically-mediated sulfate reduction. Non-carbonate contributors to alkalinity include hydroxide, silicate, borate, and organic compounds. Alkalinity helps to buffer natural water so that the pH is not greatly altered by addition of acid. The average pH of groundwater in the Study Area is slightly alkaline (Table J-1).

5.7 Groundwater Age Estimation

Groundwater age (time since recharge) was estimated based on measured ^{14}C and ^{3}H activities in the groundwater samples. Groundwater age is termed “apparent groundwater age,” because an age is calculated on the basis of simplifying assumptions regarding transport processes that can affect tracer concentrations in an aquifer. The piston-flow model is a simple and commonly used method for calculating groundwater age that assumes that the tracer moved through the aquifer in a piston-flow manner and is not altered by mixing or dispersion from the point of recharge to the point of measurement (Rupert and Plummer, 2004). However, all groundwater pumped from a well is, to some extent, mixed within the well bore. Wells with long screened intervals can draw water of different ages from multiple parts of an aquifer, where it mixes in the well bore. The mixing of water in the well bore produces mixed groundwater ages.

Measurement of stable hydrogen and oxygen isotopes in water are a useful tool to examine the recharge history of groundwater, because hydrogen and oxygen are part of the water molecule and generally are not affected by processes that may affect dissolved constituents (Kendall and McDonnell, 1998). Isotope ratios in groundwater samples that plot along the reference lines (local or global) are assumed to have originated from rainfall or snowmelt and were not affected by other isotope fractionation processes. The meteoric water line defined based on the oxygen and hydrogen stable isotopes, which includes vapor sources, ocean water, seasonal variation, weather/climate, and similar processes, is presented on Figure 5-20 (Appendix B). Globally, the stable isotopic composition of precipitation can be described by the equation:

$$\delta D = 8\delta^{18}O + 10$$

Stable-isotope ratios of hydrogen and oxygen in water reflect the altitude, latitude, and temperature of precipitation and the extent of evaporation of the water in surface water bodies or soils prior to infiltration into the aquifer. These data aid in the interpretation of the sources of groundwater recharge. Reported carbon isotopes ($\delta^{13}C$ and $\delta^{14}C$) are relative to Vienna Pee Dee Belemnite (VPDB), and deuterium (δD) and oxygen isotopes ($\delta^{18}O$) are reported relative to Standard Mean Ocean Water (SMOW). Measurement was performed using isotope-ratio mass spectrometry (IRMS). Detailed processes and procedures are provided in Appendix J.

The measured δD values in groundwater samples from the Study Area, including groundwater samples from the USGS GAMA program, ranged from -63.8 to -46.5‰ with an average value of -56.7‰ while that of δ18O ranged from -9.62 to -7.3‰ with an average of -7.9‰ (Table J-3). The results are plotted with the global meteoric water line (GMWL) on Figure 5-21 (Appendix B).

The stable isotope composition of groundwater in the Study Area is generally depleted in both δ18O and δD with respect to the GMWL. The stable isotope composition of Study groundwater and groundwater from USGS GAMA program are generally similar. In the δD and δ18O diagram (Figure 5-21 and Figure 5-22), the distribution of data points indicates that the groundwater is of meteoric origin and has been affected by evaporation. This is indicated by the fact that deuterium excess (d-excess), calculated from the relation d = δD – 8δ18O, ranges from -0.70‰ to 13.5‰ (Table J-2). The deuterium excess reflects the conditions that lead to kinetic isotope fractionation between water and vapor during the primary evaporation process. As δ18O increases (becomes more enriched), the deuterium excess in all the samples decreases gradually as shown on Figure 5-22. The low d-excess observed in the Study Area is probably related to enrichment due to kinetic evaporation and the influence of other physical factors such as duration of rainfall (amount effect) and latitude-altitude effects (Clark and Fritz, 1997). Therefore, the observed isotopic signature of the groundwater is primarily a reflection of that of the infiltrating precipitation water.Tritium (^{3}H) activities provide information about the age of groundwater. Tritium is a naturally occurring radioactive isotope of hydrogen that has a half-life of 12.43 years. It is a short lived radioactive isotope of hydrogen that is incorporated into the water molecule. Low levels of tritium are produced continuously by interaction of cosmic radiation with the Earth's atmosphere, and a large amount of tritium was produced as a result of atmospheric testing of nuclear weapons from 1952 to 1963. In this investigation, tritium was measured in Tus: one TU is equivalent to one tritium atom in 10^{18} atoms of hydrogen (Taylor and Roether, 1982). Because tritium is part of the water molecule, tritium is not affected by reactions other than radioactive decay; therefore, tritium is an excellent tracer of the movement of ground water recharged less than 50 years before present. Concentrations of tritium greater than background levels generally indicate the presence of water recharged after the early 1950s. Additional information regarding tritium analysis and results is provided in the University of Miami reports in Appendix J.

Tritium concentration alone cannot be used to quantitatively date groundwater, but can be used to qualitatively assess whether groundwater is modern (less than 50 years in age) or pre-modern (older than about 50 years in age). If a sample contains measurable tritium above 0.1 TU, then it has some post 1950s water. One cannot determine how much modern and old water is present; only the absence or presence of modern water.

As shown in Table J-2, the concentration profile of tritium in Study Area samples has a narrow range of values (from 1.14 to 2.82 TU). This narrow range of tritium enrichment maybe due to of recharge inputs from rainwater (that is, mixing with meteoric water). But the tritium activities of the drilling fluid and source water have similar magnitude as the groundwater samples. During groundwater sampling, the turbidity was high in most groundwater samples except in the day 2 and day 3 samples from Core Hole ALT B3 at 2015-2035 ft bgs. The groundwater samples may therefore be impacted by residual drilling fluid, and the tritium and carbon-14 values shown in Table J-2 may reflect the result of mixing of waters. In addition, although the day 3 sample for Core Hole ALT B3 at 2015-2035 ft bgs has the lowest tritium value (1.14 TU), this value is still above the indicated threshold of 0.1 TU, so this sample may have been impacted by drilling fluids or the sampling methodology (e.g., potential exposure to air).

Concentrations of tritium for the data reported by USGS GAMA program for the Study Area are higher than the values of the current study as discussed in the results section. Tritium activities from these four wells (GAMA-SG-03, GAMA-SG-08, GAMA-SG-21, and GAMA-SG-24) may accurately reflect the presence of post-1952 groundwater recharge. But in the absence of information on the specific depth from which the USGS GAMA samples were collected, a proper evaluation and assessment of the results cannot be made.

Low levels of ^{14}C are produced continuously by interaction of cosmic radiation with the Earth's atmosphere and are incorporated into atmospheric carbon dioxide. Carbon dioxide dissolves in precipitation, surface water, and groundwater exposed to the atmosphere, thereby entering the hydrologic cycle. Because ^{14}C decays with a half-life of approximately 5,700 years, low activities of ^{14}C, relative to modern values, generally indicate groundwater that is several thousand years old or more. For ^{14}C, the apparent groundwater age would illustrate the residence time of the water in the absence of any hydro-geochemical effects. The best illustration of age would have to be derived by incorporating the radiocarbon pMC or F^{14}C result into models that take the hydrologic conditions of the aquifer into account. The apparent radiocarbon age is used as a relational tool to interpret hydrologic differences between wells and to monitor temporal changes. Detailed processes and procedures are provided in Appendix J.

Carbon-14 activities provide information about the age (time since recharge) of the groundwater. In general, carbon-14 activities were higher in the deep water than in the shallow water (Table J-2) as shown on Figure 5-23 (Appendix B).

Despite potential impact by drilling fluid, the general decrease in carbon-14 activity with depth suggests that deep water is older than shallow water, as expected. Furthermore, the oldest estimated carbon-14 age of 4520 years is for the sample purged for the longest time and considered least impacted by drilling fluid, the day 3 sample for Core Hole ALT-B3 at 2015-2035 ft bgs. While this estimated age may not be accurate, a significantly greater groundwater age and change in geochemistry with depth is indicated.

Overall, lower carbon-14 activities and lower tritium activities correlate with increased depth of samples as shown on Figure 5-24 (Appendix B), suggesting increasing groundwater age with depth. The carbon-14 and tritium activities for the USGS GAMA sampling program indicate younger water (Figure 5-24).

The results of the geochemical, stable isotopes (oxygen, hydrogen, and carbon), and radioactive isotopes (carbon-14 and tritium) investigation in the Study Area suggest that the shallow and deep groundwater are hydrogeologically separated and/or that downward vertical movement of groundwater is slow, and the age of groundwater at the deepest proposed tunnel depths may be several thousand years.

5.8 In-Situ Stresses

In-situ stress determination testing was performed at Core Hole E1-B1 and ALT-B3 to estimate the Maximum and Minimum Horizontal Stress (σ_H, σ_h, respectively) and their orientations (reported as trends). Previously, Table 3-6 summarized the results.

In-situ stress determination testing in four of the tests at Core Hole E1-B1 indicates a Northwest-Southeast (111-291 to 158-338 degrees) orientation for the maximum horizontal stress. The orientation obtained from the testing from core depth 2,324.7 to 2,332.0 feet, is 061-241 degrees (Northeast-Southwest) counter to the general trend. but may be influenced by the presence of granitic dikes in the tested zone. Figure 5-25 (Appendix B) presents an interpreted depth versus stress profile. A least-squares linear regression of the testing results in pressure gradients of 0.84 and 0.71 pounds per square inch per foot (psi/ft) for the maximum and minimum horizontal stress, respectively. Assuming the vertical lithostatic stress is a principal stress and has a gradient of about 1.25 psi/ft, the ratio of the maximum and minimum horizontal stress to the vertical stress (σ_H / σ_v and σ_h / σ_v) are 0.67 and 0.57, respectively.

In-situ stress determination testing at Core Hole ALT-B3 indicates a Northwest-Southeast (137-324 to 144-317 degrees) orientation for the maximum horizontal stress. Figure 5-26 (Appendix B) presents an interpreted depth versus stress profile. A least-squares linear regression of the testing results in pressure gradients of 1.47 and 1.11 pounds per square inch per foot (psi/ft) for the maximum and minimum horizontal stress, respectively. Assuming the vertical lithostatic stress is a principal stress (i.e., the intermediate principal stress) and has a gradient of about 1.20 psi/ft, the maximum and minimum horizontal stress coefficients (σ_H / σ_v and σ_h / σ_v) are 1.23 and 0.93, respectively. The stress field at Core Hole ALT-B3, which appears to be non-gravitational, is likely a result of the core hole's close proximity to the San Gabriel fault.

5.9 Laboratory Testing

Laboratory test results can be grouped into testing performed for rock mechanics, tunnel boring machine (TBM) design, and swelling classification. Appendix I presents laboratory test results.

5.9.1 Rock Mechanics

Rock mechanics is a branch of engineering that deals specifically with the mechanical properties and behavior of rock mediums. At most project scales, rock mediums are comprised of intact blocks of rock separated by discontinuities. This complex medium is commonly referred to simply as rock mass. Testing performed on small-diameter rock cores is not representative of rock mass. However, testing is necessary to establish input parameters required by empirical rock mass classification or characterization systems, input parameters for Hoek-Brown criterion, or to establish other mechanical properties of intact rock. In competent rock mass, use of the Hoek-Brown criterion is typically the standard of practice. However, in relatively thick zones (i.e., compared to the scale of excavation) of weak to extremely weak (Rock Grades R0 to R2) rock, massive intact rock, or fine- to coarse-grained intermediate geomaterials (i.e., materials that are neither soil nor rock), small-scale testing and use of Mohr-Coulomb or other shear strength criterions may accurately model rock and tunnel structure interactions.

5.9.1.1 Intact Rock Strength

One of the most important and common input parameters to rock mass classification systems is the intact rock strength or uniaxial (unconfined) compressive strength of intact rock (σ_c). The point load index [$I_{s(50)}$] and Brazilian (in-direct tensile splitting) tensile strength (σ_t) are indicative of intact rock strength and can be correlated to σ_c. Intact rock strength results can be summarized using the International Society for Rock Mechanics' (ISRM) Rock Grade (1978) descriptors and ranges (Table 5-3). The individual test reports are included in Appendix I. Presumptive correlations between the test methods are described in Table 5-3 and compared in Figure 5-27 (Appendix B). Based on the variability inherent in rock mechanics testing, these presumptive correlations are used only as an index of intact rock strength and not as actual design values. For selecting an appropriate design value, site specific conditions, lithology, and test method should be considered.

Histograms of intact rock strength testing for each core hole and the lithologies tested are included as Figure 5-28 through Figure 5-32 (Appendix B). For point load and Brazilian testing where a representative value is reported from the average of several breaks, these histograms consider each break and do not discard high and low values.

Table 5-3 Rock Grade and Intact Rock Strength

Rock Grade	Descriptor	Unconfined Compressive (σ_c)	Point Load[1] [$I_{s(50)}$]	Brazilian Tensile[2] (σ_t)
		MPa		
R0	extremely weak	0.25-1.0	0.01-0.04	0.02-0.1
R1	very weak	1.0-5.0	0.04-0.20	0.1-0.5
R2	weak	5.0-25	0.20-1	0.5-2.5
R3	medium strong	25-50	1-2	2.5-5
R4	strong	50-100	2-4	5-10
R5	very strong	100-250	4-10	10-25
R6	extremely strong	>250	>10	>25

Source: Adapted from ISRM, 1978

[1] A linear constant (k) for correlating point load strength to unconfined compressive strength is typically presumed as 24. For weak rock lithologies, some researchers have used a linear constant as low as 10.

[2] A linear constant (k) for correlating Brazilian tensile strength to unconfined compressive strength is typically presumed as 10.

5.9.1.2 Discontinuity Shear Strength

A total of 17 select natural rock discontinuities occurring within the rock cores were tested to establish discontinuity shear strengths that are useful in tunnel stability and design analyses. The shear strength of rock discontinuities is highly variable and depends on numerous factors (i.e., roughness, aperture, infill material, weathering of joint surfaces, in-situ water pressure, shear-rate, etc). Discontinuity shear strength is typically defined using a Mohr-Coulomb or Barton-Bandis shear strength criterion. Figure 5-33 (Appendix B) presents the direct shear test results, lithology, joint roughness coefficients (JRC), and weathering conditions for the rock cores tested.

Assuming a nominal cohesion, which is applicable to un-healed and other cohesionless discontinuities, the peak discontinuity shear strengths are bounded by lower and upper discontinuity frictions angles (ϕ_{peak}) of 19 to 50 degrees, respectively. Similarly, the ultimate discontinuity shear strengths are bounded by lower and upper discontinuity friction angles (ϕ_{ult}) of 18 to 37 degrees, respectively. The discontinuities within anorthosite define the higher bound shear strengths. The lower bound is defined by a discontinuity within gabbro obtained from Core Hole E1-B1 at core depth 1,617.5 feet.

5.9.1.3 Triaxial Testing

Triaxial testing (i.e., triaxial compressive strength) of rock core is performed to establish triaxial compressive strength or elastic properties under confinement. The triaxial test results are useful for establishing Hoek-Brown parameters [i.e., the material constant (m_i)] for lithologies that may not be represented in Hoek's laboratory testing database (Marinos and Hoek, 2000) or for establishing Mohr-Coulomb shear strength or other shear strength parameters for intermediate geomaterials.

We consider the anorthosite as a rock type unlikely (unique mineral composition, geologic history and occurrence) to be represented in Hoek's database. Therefore, triaxial tests on rock cores of anorthosite were performed to establish representative m_i. Based on analysis of triaxial and uniaxial compressive testing of cores collected from Core Hole E1-B1, we estimate an m_i of 11 for anorthosite using the method published by Hoek (2007). This m_i is less than what might be inferred from published values (Marinos and Hoek, 2000) for light-colored plutonic igneous rock types, with m_i reportedly ranging from 20 to 35.

Gouge, breccia and sheared zones comprised of weakly lithified, very dense mixtures of clay to fine-gravel size rock fragments are considered intermediate geomaterials. Triaxial testing of intermediate geomaterials from core holes FS-B1, E1-B2 and ALT-B2 was completed to establish Mohr-Coulomb shear strength parameters. Attempts to add moisture to several samples were unsuccessful and resulted in sample degradation that rendered them unsuitable for testing. Thereafter, the remaining samples were tested at the moisture as-received by the laboratory. Figure 5-34 (Appendix B) presents Mohr-Coulomb circles for testing completed on intermediate geomaterials. The test results are bounded by:

- Upper bound
  internal friction angle (ϕ) = 40 degrees
  cohesion (c) = 825 pounds per square inch (psi)
  tensile strength (σ_t) = 400 psi
- Lower bound
  ϕ = 24 degrees
  c = 0 psi
  σ_t = 0 psi

Use of test data plotted on Figure 5-34 should consider an appropriate Mohr-Coulomb shear strength representative of the core hole location and lithology.

5.9.1.4 Slake Durability

Slaking is a broad term used to describe rock deterioration resulting from exposure during construction. The Slake Durability Index developed by Franklin and Chandra (1972) and Gamble (1971) is an index of rock susceptibility to slaking. Slake durability tests were performed on limited select core samples and rock lithologies that were prone to crumbling when handled or wetted. Table 5-4 summarizes the limited slake durability index testing performed.

Table 5-4 Slake Durability Index Test Results

Core Hole	Rock Unit	Lithology	Core Depth[1]		2nd Cycle Slake Durability Index [$I_{d(2)}$]	Group Name[2]
			feet			
FS-B1	Fault Zone	breccia	394.8	395.7	34	low durability
E1-B1	Anorthosite	anorthosite (inclusion)	2,666.2	2,667.1	93	med. to high durability
E1-B2	Granodiorite	granodiorite (sheared)	310.7	310.9	50	low durability
E1-B2	Granodiorite	granodiorite (sheared)	673.3	673.8	89	med. to high durability
ALT-B2	Gneiss	gneiss (brecciated)	496.5	497.2	97	high durability
ALT-B2	Granodiorite	flaser granite	1,428.4	1,428.8	84	medium durability

[1] Test intervals reported are core depths not vertical depths, and do not include corrections for core hole plunge.

[2] The reported durability group name is based on the group established by Gamble (1971).

5.9.2 Parameters Related to Tunnel Boring Machine Design

Tunnel boring machine (TBM) design requires additional considerations aside from intact rock strength. Limited punch penetration and Cerchar Abrasiveness Index (CAI) testing, and petrographic analyses were completed to provide data for TBM design.

The punch penetration test simulates tool penetration necessary to excavate (chip) hard rock and is an index of rock resistance to excavation. The resulting peak slope indices are summarized in Table 5-5. The punch penetration results along with others parameters can be used by the TBM designer in Colorado School of Mines TBM performance prediction models (Rostami, 1991; Rostami and Ozdemir, 1993).

Table 5-5 Tunnel Boring Machine Design Test Results

Core Hole	Rock Unit	Lithology	Core Depth[1]		Peak Slope Index	CAI	Abrasiveness[2]
			feet		kips/inch		
FS-B1	Anorthosite	anorthosite	873.5	874.7	242	3.6	high
E1-B1	Anorthosite	gabbro	850.5	851.5	224	3.7	high
E1-B1	Anorthosite	granitic rock	2,282.7	2,283.4	222	4.6	extreme
E1-B1	Anorthosite	anorthosite	2,335.4	2,336.7	257	4.3	extreme
ALT-B2	Granodiorite	flaser granite	1,511.0	1,511.9	93	2.9	high
ALT-B3	Granite	granite	2,005.3	2,006.0	193	4.5	extreme
ALT-B3	Granite	granite	2,020.0	2,021.0	246	4.7	extreme

[1] Test intervals reported are core depths not vertical depths, and do not include corrections for core hole plunge.

[2] The reported Cerchar Abrasivity Index is based on Rockwell Hardness Scale (HRC) 55 test pins and the criteria from Table 1 in ASTM D7625.

Predicting the wear of tooling during excavation in rock is critical for planning purposes and TBM design. The CAI test results are summarized in Table 5-5. Table 5-6 summarizes weighted Moh's hardness and quartz content from petrographic analysis, which are indicative of abrasive rock conditions.

Table 5-6 Summary of Quartz Content and Weighted Moh's Hardness

Core Hole	Rock Unit	Lithology	Core Depth[1]		Quartz Content	Weighted Moh's Hardness[2]
			feet		%	
FS-B1	Syenyite	syenite	248.7	249.1	5	5.7
FS-B1	Fault Zone	breccia	368.0	368.3	0	3.4
FS-B1	Anorthosite	gabbro	821.5	821.7	0	5.5
FS-B1	Anorthosite	anorthosite	869.3	869.7	0	6.2
FS-B1	Anorthosite	gabbro	904.0	904.3	0	5.4
E1-B1	Anorthosite	gabbro (leuco)	113.7	114.0	10	6.1
E1-B1	Anorthosite	gabbro (chloritized)	262.4	262.8	1	2.2
E1-B1	Anorthosite	anorthosite	1,086.2	1,086.6	5	6.2
E1-B1	Anorthosite	granitic (vein)	1,529.0	1,529.5	9	5.3
E1-B1	Anorthosite	granitic (pegmatite)	1,976.8	1,977.0	25	6.4
E1-B1	Anorthosite	granitic (vein)	2,083.0	2,083.5	42	6.4
E1-B1	Anorthosite	anorthosite	2,175.5	2,175.9	1	6.1
E1-B1	Anorthosite	granitic (vein)	2,597.0	2,597.5	45	6.5
E1-B1	Anorthosite	anorthosite	2,692.8	2,693.1	2	6.2
E1-B2	Granodiorite	granite	180.4	180.8	32	6.4
E1-B2	Granodiorite	granodiorite	422.9	423.4	26	6.0
E1-B2	Granodiorite	granodiorite (sheared)	663.1	663.2	15	4.6
E1-B2	Granodiorite	granodiorite (sheared)	673.8	674.2	7	4.6
E1-B2	Granodiorite	granodiorite	709.2	709.6	25	6.1
E1-B2	Granodiorite	granite	950.0	950.5	32	6.4
ALT-B2	Gneiss	gneiss (brecciated)	742.6	743.3	0	5.9
ALT-B2	Gneiss	gneiss	861.0	861.3	40	6.0
ALT-B2	Fault Zone	fault breccia/gouge	1,062.0	1,062.8	13.0	3.6
ALT-B2	Granodiorite	flaser granite	1,343.0	1,343.5	25	6.0
ALT-B2	Fault Zone	fault breccia/gouge	1,543.2	1,544.5	17.0	3.7
ALT-B2	Fault Zone	fault breccia/gouge	1,581.5	1,582.2	21.0	3.9
ALT-B3	Granodiorite	granite	274.0	274.3	40	6.3
ALT-B3	Granodiorite	gabbro	849.9	850.1	0	5.7
ALT-B3	Granodiorite	granite	880.7	881.1	25	6.4
ALT-B3	Granodiorite	granodiorite	1,028.3	1,028.6	30	6.3
ALT-B3	Granodiorite	granodiorite	1,377.0	1,377.5	20	3.8
ALT-B3	Granodiorite	granodiorite	1,517.4	1,517.7	27	6.0

Core Hole	Rock Unit	Lithology	Core Depth[1]		Quartz Content	Weighted Moh's Hardness[2]
			feet		%	
ALT-B3	Granite	granite (gouge)	1,975.2	1975.4	38	4.4
ALT-B3	Granite	granite	1,996.8	1,997.1	39	6.5

[1] Test intervals reported are core depths not vertical depths, and do not include corrections for core hole plunge.
[2] The weighted Moh's hardness is based on the relative cross-sectional area of the minerals observed using optical method, and by relative abundance where reported from X-ray powder diffraction analysis.

5.9.3 Swelling Classification

Swelling is a term used to describe the phenomenon where clay or other minerals (e.g., smectite, montmorillinite, vermiculite, anhydrite, pyrrhotite, etc.) absorb water into their mineralogical structures and increase in volume. Where swelling zones are restrained, large pressures may ensue. Important considerations for evaluating swell include clay mineralogy, plasticity, moisture conditions, degree of consolidation, and tunneling method. With respect to the five locations explored, gouge and fine-grained infill was most prevalent within rock types observed from Core Holes E1-B2 and ALT-B2. Swelling classification tests included geotechnical laboratory testing, and X-ray diffraction (XRD) analysis.

Table 5-7 summarizes the geotechnical laboratory testing of intermediate geomaterials (gouge and infill in shear zones) sampled from Core Hole E1-B2 and ALT-B2. Testing methods included moisture content, particle-size analysis, Atterberg Limits, and consolidation (swell potential) testing.

Sample moisture was not preserved for rock cores obtained at Core Hole E1-B2. Particle-size analyses and Atterberg Limits testing in five sheared zones (core depths 368, 438, 491, 639, and 662 feet) resulted in Unified Soils Classification System (USCS) groups ranging from Silty SAND (SM) to SAND with Silt (SP-SM or SW-SM). The Atterberg Limits testing on four samples from Core Hole E1-B2 were non-plastic (NP).

Because of the observed clay content in the field of the brecciated lithologies and gouge, methods to preserve sample moisture and expedite testing were implemented for samples collected from Core Hole ALT-B2. Two samples of intermediate geomaterial tested from shear zones at core depths 498 and 1,058 feet resulted in USCS groups of sandy Lean CLAY (CL) and sandy Fat CLAY (CH), respectively. Hydrometer analyses and Atterberg Limits testing was completed on these samples to estimate the activity (A) and liquidity index (LI). Based on the limited testing, the LI indicate heavily overconsolidated "soil" that may be desiccated or highly expansive (FHWA, 2002). Figure 5-35 (Appendix B) presents published correlations that indicate these intermediate geomaterials include mixtures of montmorillonite (calcium) and illite and have a Low to Medium swelling potential (less than 5 percent) according to Seed et al. (1962). Consolidation testing on clay-rich material from core depth of 1,058 feet indicate a swell pressure (i.e., pressure required for zero positive vertical strain upon wetting) of 183 pounds per square inch (psi). It should be noted this result is from a single test and may not be representative of the entire range of swell pressures encountered during tunneling within these materials.

Table 5-7 Summary Geotechnical Laboratory Testing of Gouge and Infill Materials

Core Hole	Rock Unit	Lithology	Core Depth[1]		Dry Unit Wt.	Moist. Content	Gravel	Sand	Fines	Liq. Limit	Plasti. Index	Liq. Index	Activity	Swell Press.
			feet		pcf	%	%							psi
E1-B2	Granodiorite	granodiorite (sheared)	368.0	368.3	--	--	--	--	24	--	--	--	--	--
E1-B2	Granodiorite	granite (sheared)	262.4	262.8	--	--	--	--	17	--	NP	--	--	--
E1-B2	Granodiorite	granodiorite (sheared)	663.1	663.2	--	--	2	63	35	--	NP	--	--	--
E1-B2	Granodiorite	granite (sheared)	673.8	674.2	--	--	--	--	11	--	NP	--	--	--
E1-B2	Granodiorite	granodiorite (sheared)	1,062.0	1,062.8	--	--	--	--	31	--	NP	--	--	--
ALT-B2	Gneiss	gneiss (brecciated)	498.3	499.5	110.4	18.2	3	47	50	16	54	-0.2	1.9	--
ALT-B2	Fault Zone	breccia/gouge	1,057.3	1,057.8	136.1	9.1	1	31	68	30	41	-0.2	0.9	183
ALT-B2	Fault Zone	breccia/gouge	1,545.3	1,547.8	--	--	7	28	65	9	23	--	1.1	--

[1] Test intervals reported are core depths not vertical depths, and do not include corrections for core hole plunge.

XRD petrographic methods (Appendix E) were used to identify clay mineralogy of fines as infill material in shears and as matrix comprising fault breccia and gouge. Table 5-8 summarizes the predominant clay mineralogy from the limited XRD testing. Potential swelling clays (i.e., montmorillonite, and smectite) were identified in XRD testing of samples from Core Holes FS-B1, E1-B1, ALT-B2 and ALT-B3.

Table 5-8 Summary of XRD and Clay Mineralogy

Core Hole	Rock Unit	Lithology	Core Length Depth[1]		Predominant Clay Mineral	Relative Content
			feet			%
FS-B1	Fault Zone	breccia	368.0	368.3	chlorite/smectite	35
E1-B1	Anorthosite	gabbro (chloritized)	262.4	262.8	montmorillonite	55
E1-B2	Granodiorite	granodiorite (sheared)	663.1	663.2	chlorite	30
E1-B2	Granodiorite	granodiorite (sheared)	673.8	674.2	chlorite	31
ALT-B2	Fault Zone	fault breccia/gouge	1,062.0	1,062.8	montmorillonite	44
ALT-B2	Fault Zone	fault breccia/gouge	1,543.2	1,544.5	illite/smectite	31
ALT-B2	Fault Zone	fault breccia/gouge	1,581.5	1,582.2	chlorite	25
ALT-B3	Granodiorite	granodiorite	1,377.0	1,377.5	chlorite	6
ALT-B3	Granite	granite (gouge)	1,975.2	1975.4	montmorillonite	28

[1] Test intervals reported are core depths not vertical depths, and do not include corrections for core hole plunge.

5.10 Rock Mass Characterization

The following rock mass characterization/classifications including:

- Deere's (1964; 1989) Rock Quality Designation (RQD);
- Bieniawski's (1989) Rock Mass Rating (RMR);
- Hoek et al.'s (1995) Geological Strength Index (GSI), and
- Barton et al.'s (1974; 1994) Rock Mass Quality (Q).

The rock mass characterization results for the various rock intervals within each of the ANF core holes are plotted on Figure 3-1 through Figure 3-16. Appendix K includes additional information regarding the rock mass characterization.

5.10.1 Rock Quality Designation (RQD)

The depth versus RQD for the ANF core holes are plotted along with other rock mass data on Figure 3-1 through Figure 3-16 and summarized for each core hole location as histograms in Figure 5-36 through Figure 5-40 (Appendix B). Appendix K includes additional information about RQD. As summarized in Table 5-9, Deere (1989) uses several descriptors to define rock quality using RQD.

Table 5-9 RQD Descriptors

RQD (%)	Rock Quality
0-25	Very Poor
25-50	Poor
50-75	Fair

RQD (%)	Rock Quality
75-90	Good
90-100	Excellent

At Core Hole FS-B1, the length-weighted RQD is at the threshold between Fair and Good (75) and the RQD are unevenly distributed predominantly between Fair to Excellent when considering all rock types. RQD for core runs of anorthosite and gabbro are predominantly Fair to Excellent. RQD for core runs of syenite, syenite with gabbro, and lithologies within the fault zone are more unevenly distributed between the Poor to Excellent RQD ranges.

At Core Hole E1-B1, the length weighted RQD is Good (81) and the RQD are distributed predominantly between Fair to Excellent when considering all rock types. RQD for core runs of anorthosite are predominantly Good to Excellent. RQD for core runs of leucogabbro and gabbro, and granitic rock are more widely distributed.

At Core Hole E1-B2, the length weighted RQD (62) and modal RQD when considering all rock types is Fair. The RQD for all of the rock types at this location are nearly normally distributed from Very Poor to Excellent, with the exception of rock types within the fault zone, which are bi-modally distributed between Poor and Excellent.

At Core Hole ALT-B2, the length weighted RQD (46) is Poor and the modal RQD is Very Poor when considering all rock types. In general, RQD varies widely at this core hole location; however, the rock lithologies are predominantly Very Poor to Fair with the exception of the gneiss, which is predominantly Fair to Good.

At Core Hole ALT-B3, the length weighted RQD (58) and mode when considering all rock types is Fair. The RQD are nearly normally distributed for the various rock lithologies at this location.

5.10.2 Rock Mass Rating (RMR)

Basic Rock Mass Ratings (RMR_{basic}), which do not include the adjustment factor (R_A), were estimated using the gINT database and project data included in this report (e.g., laboratory testing, instrumentation, etc). For locations where it is feasible to project core holes to the tunnel envelope (i.e., Core Hole ALT-B2 and ALT-B3), R_A are provided in tabular format within Appendix K. The core depth versus RMR_{basic} are plotted on Figure 3-1 through Figure 3-16 and summarized for populations from each core hole location as histograms in Figure 5-41 through Figure 5-45 (Appendix B). As summarized in Table 5-10, Bieniawski (1989) uses several descriptors to define rock mass class using RMR.

Table 5-10 RMR Rock Mass Class Descriptors

RMR	Rock Classes	Description
0-20	I	Very Poor
21-40	II	Poor
41-60	III	Fair
61-80	IV	Good
81-100	V	Very Good

At Core Hole FS-B1, the population of RMR_{basic} are distributed nearly normally between Very Poor and Good, with a mode of Fair. For rock lithologies within the fault zone, the population of RMR_{basic} are bi-modally distributed about mode Poor and Fair.

At Core Hole E1-B1, the population of RMR_{basic} are distributed nearly normally between Poor and Good with a mode of Fair. The distribution is slightly skewed toward Good.

At Core Holes E1-B2 and ALT-B2, the population of RMR_{basic} are bi-modally distributed with modes of Poor and Fair. These results are presumably strongly affected by the proximity of these core holes to the San Gabriel fault.

At Core Hole ALT-B3, the population of RMR_{basic} are nearly normally distributed between Very Poor and Good and has a mode of Fair. The distribution is slightly skewed toward Poor by the granodiorite and mixed granite and granodiorite lithologies.

5.10.3 Geological Strength Index (GSI)

Geological Strength Indices (GSI) were estimated using the gINT database and project data included in this report (e.g., laboratory testing, instrumentation, etc). The core depth versus GSI are plotted on Figure 3-1 through Figure 3-16 and summarized for each core hole location as histograms in Figure 5-46 through Figure 5-50 (Appendix B). For GSI, the same rock mass classes and descriptors as those summarized for RMR in Table 5-10 are used. Because of the strong relation between RMR and GSI, the trends at each location are similar to those discussed previously for RMR_{basic}. In general, the GSI values are higher (i.e., distributions are shifted toward Good and Very Good) than those predicted by RMR, because GSI does not factor in site-specific conditions like groundwater and joint orientation.

5.10.4 Rock Mass Quality (Q)

Rock Mass Qualities (Q) were estimated using the gINT database and project data included in this report (e.g., laboratory testing, instrumentation, etc). The core depth versus RMR correlated from Q are plotted on Figure 3-1 through Figure 3-16 and summarized for each core hole location as histograms in Figure 5-51 through Figure 5-55 (Appendix B). For Q, rock classes and descriptors defined by Barton et al. (1974 and 1994) are summarized in Table 5-11.

Table 5-11 Q Class Descriptors

Q	Rock Classes	Description
0.001-0.004	G	Exceptionally Poor
0.004-0.1	F	Extremely Poor
0.1-1	E	Very Poor
1-4	D	Poor
4-10	C	Fair
10-40	B	Good
40-100	A	Very Good
100-400	A	Extremely Good
400-1000	A	Exceptionally Good

At Core Hole FS-B1, the population of Q are skewed toward Fair and Good with a mode of Poor. For syenite, the population of Q is distributed between Extremely Poor to Good, has a mode of Good, and is skewed toward Good.

At Core Hole E1-B1, the population of Q considering all rock types from the anorthosite complex are skewed toward the Extremely Poor to Poor classes of the histogram with a mode of Very Poor. The estimated Q for Core Hole E1-B1 are negatively impacted by the abundance of discontinuities within the rock mass, and the high in-situ stress and groundwater pressures.

At Core Holes E1-B2, ALT-B2 and ALT-B3, the population of Q are skewed toward the Extremely Poor to Poor classes of the histograms with a mode of Very Poor.

In general, the rock mass conditions described by Q vary more and are generally less favorable (i.e., with respect to support and stand-up) than those described using RMR. The differences are largely attributed to the following:

- Intact rock strength is not considered directly by Q, but is considered indirectly in terms of in-situ stress when estimating the stress reduction factor (SRF) for competent rock;
- In-situ stress conditions are not considered by RMR; and
- Q varies over several orders of magnitude compared with RMR, which varies from 0 to 100.

For estimating or extrapolating rock mass conditions, the effects of site-specific factors considered in either RMR or Q (e.g., R_5, R_A, SRF, and J_w) should be considered and modified as necessary.

6 REFERENCES

ASTM International (ASTM). 2016. *Annual Book of ASTM Standards.*

Atwater, T.M., 1998, *Plate Tectonic History of Southern California with Emphasis on the Western Traverse Ranges and Santa Rosa Island*: American Association of Petroleum Geologists, MP 45, pp. 1-8.

Bailey, H.P. 1966. *The Climate of Southern California*. Berkeley and Los Angeles, University of California Press.

Barnes, C.J. and G.B. Allison. 1988. *Tracing of water movement in the unsaturated zone using stable isotopes of hydrogen and oxygen*: Journal of Hydrology Volume100, Numbers 1-3, pp. 143–176.

Barrows, A.G., J.E. Kahle, R.B. Saul, and F.J. Weber Jr. 1974 *Geologic Map of the San Fernando Earthquake Area*, *in* Oakshott, G.B. (editor), San Fernando, California, Earthquake of 9 February 1971: California Division of Mines and Geology Bulletin 196, plate 2, scale 1:18,000.

Barrows, A.G., J.E. Kahle, and D.J. Beeby. 1985. *Earthquake hazards and tectonic history of the San Andreas fault zone, Los Angeles County, California*: California Division of Mines and Geology (CDMG) Open-File Report 85-10 LA, 19 plates, scale 1:12,000, 139p.

Barton, C.L. and N.N. Sampson. 1949. *Placerita Oil Field, in Summary of Operations, California Oil Fields*: California Division of Oil and Gas and Geothermal Resources (DOGGR), Volume 35, Number 2, pp. 5-14.

Barton, N.R. and E. Grimstad. 1994. *The Q-system Following Twenty Years of Application in NMT Support Selection*: Felsbau. Volume 12, Number 6, pp. 428-436.

Barton, N.R., R. Lien, and J. Lunde. 1974. *Engineering Classification of Rock Masses for the Design of Tunnel Support*: International Journal of Rock Mechanics and Mining Sciences, Volume 6, Number 4, pp. 189-239.

Bentley Software. 2016. *gINT Pro Plus, V8i version 08.03.04.285.*

Beyer, L.A., T.H. McCulloh, R.E. Denison, R.W. Morin, R.J. Enrico, J.A. Barron, J.A. and R.J. Fleck. 2009. *Post-Miocene Right Separation on the San Gabriel and Vasquez Creek Faults, with Supporting Chronostratigraphy, Western San Gabriel Mountains, California*: U.S. Geological Survey (USGS) Professional Paper 1759, 44p.

Bieniawski, Z.T. 1993. *Classification of Rock Masses for Engineering: the RMR System and Future Trends*. Comprehensive Rock Engineering, Volume 2, Chapter 22. Pergamon Press.

______. 1989. *Engineering Rock Mass Classifications.* John Wiley & Sons, New York.

Bryant, W.A. and E.W. Hart. 2007. *Fault-Rupture Hazard Zones in California, Alquist-Priolo Earthquake Fault Zoning Act with Index to Earthquake Fault Zones Maps*: California Geological Survey (CGS) Special Publication 42, 42p.

Caine J.S. and S.A. Minor. 2009. *Structural and geochemical characteristics of faulted sediments and inferences on the role of water in deformation, Rio Grande Rift, New Mexico*: Geological Society of America Bulletin, Volume 121, Number 9/10, pp. 1325–1340.

Caine J.S., S.A. Minor, V.J.S. Grauch, and M.R. Hudson. 2002. *Potential for fault zone compartmentalization of groundwater aquifers in poorly lithified, Rio Grande rift-related sediments, New Mexico*: Geological Society of America Abstracts with Programs, Volume 34, Number 4, pp. 59.

California Department of Transportation (Caltrans). 2010. *Soil and Rock Logging Classification and Presentation Manual, 2010 Edition*. Sacramento, 82p.

California Department of Water Resources (DWR). 1981. *Water Well Standards*: Bulletin 74-81, 93p.

______. 1991. *California Well Standards, Water Wells, Monitoring Wells, Cathodic Protection Wells*: Bulletin 74-90 (Supplement to Bulletin 74-81) 74p.

______. 1993. *Investigation of Water Quality and Beneficial Uses: Upper Santa Clara River Hydrologic Area*: Final Project Report.

California Geological Survey (CGS). 2002. *California Geomorphic Provinces*, Note 36, 4p.

______ (CGS). 2016. *Interactive Fault Activity Map of California, 2010*. Date accessed 4/27/16, http://maps.conservation.ca.gov/cgs/fam/.

California High-Speed Rail Authority (Authority). 2011a. Technical Memorandum 2.9.1, Geotechnical Investigation Guidelines.

______. 2011b. Technical Memorandum 2.9.2, Geotechnical Report Guidelines.

______. 2011c. Technical Memorandum 2.9.3, Geologic and Seismic Hazard Analysis Guidelines.

______. 2011d. Technical Memorandum 2.9.10, Geotechnical Analyses and Design Guidelines.

______. 2011e. Notice to Designers No. 1 – Geotechnical Investigations for Preliminary Design.

______. 2011f. Notice to Designers No. 8 – Geotechnical Boring and Sample Identification, Handling and Storage Guidelines.

______. 2014. Technical Memorandum 2.10.6, Fault Rupture Analysis and Mitigation.

______. 2015a. *Engineering Report, 15% Draft Palmdale to Burbank, Fault Hazard Evaluation Report.* Prepared by HMM/URS/Arup RC, dated June 2015.

______. 2015b. *Engineering Report, 15% Draft Palmdale to Burbank, Historic Geotechnical Data Report.* Prepared by HMM/URS/Arup RC, dated June

______. 2015c. Preliminary Geophysical/Geotechnical Investigation Plan for Proposed Tunnel Alternatives in Angeles National Forest, EEPB-KLF-TK04-0001-05, August 21, 2015, 248 pages.

______. 2016a. *Core Hole FS-B1, Proposed Laboratory Testing Program Memorandum EEPB-KLF-TK04-ME0002_REV00.* Prepared by Kleinfelder, March 28, 2016.

______. 2016b. *Core Hole E1-B2, Proposed Laboratory Testing Program Memorandum EEPB-KLF-TK04-ME0003_REV00.* Prepared by Kleinfelder, April 22, 2016.

______. 2016c. *Core Hole E1-B1, Proposed Laboratory Testing Program Memorandum EEPB-KLF-TK04-ME0018_REV00.* Prepared by Kleinfelder, June 9, 2016.

______. 2016d. *Core Hole ALT-B2, Proposed Laboratory Testing Program Memorandum EEPB-KLF-TK04-ME0021_REV00.* Prepared by Kleinfelder, July 12, 2016.

______ 2016e. *Core Hole ALT-B3, Proposed Laboratory Testing Program Memorandum EEPB-KLF-TK04-ME0026_REV00.* Prepared by Kleinfelder, September 7, 2016.

Campbell, R.H., C.J. Willis, P.J. Irvine, and B.J. Swanson. 2014. *Preliminary Geologic Map of the Los Angeles 30'x60' Quadrangle, California*, version 2.1: California Geological Survey (CGS), Scale 1:100,000.

Cao, T. W.A. Bryant, B. Rowshandel, D. Branum, and C.J. Wills. 2003. *The Revised California Probabilistic Seismic Hazard Maps, June 2003*: California Geological Survey (CGS), available at: http://www.conservation.ca.gov/cgs.

Carter, Bruce. 1980a. *Structure and Petrology of the San Gabriel Anorthosite-Syenite Body, Los Angeles County, California*: Dissertation (Ph.D), California Institute of Technology, 393p.

______. 1980b. *Field Trip Guide to the Anorthosite-Syenite Terrain of the Western San Gabriel Mountains, Los Angeles County, California: with Emphasis on the Origin of the Layered Gabbroic Rock*: prepared for the National Association of Geology Teachers--Far Western Section meeting at Pasadena City College, Pasadena, California, April, 1980, 48p.

______. 1982. *Geology and Structural Setting of the San Gabriel Anorthosite-Syenite Body and Adjacent Rocks of the Western San Gabriel Mountains, Los Angeles County, California*, *in* Cooper, J.D. (compiler), Geological Society of America, Cordilleran Section, Field Trip Number 5; Geologic Excursion in the Transverse Ranges, Southern California, Guidebook, pp. 1-53.

Clark, I., and P. Fritz, 1997. *Environmental Isotopes in Hydrogeology*, Lewis Publishers, Boca Raton.

Cotton, W.R. 1986. *Holocene Paleoseismology of the San Gabriel fault, Saugus/Castaic area, Los Angeles County, California:* Geological Society of America, 82nd annual meeting of the Cordilleran Section, California State University at Los Angeles, pp. 33–41.

Cotton, William and Associates, Inc. 1985. *Holocene Behavior of the San Gabriel Fault, Saugus/Castaic Area, Los Angeles County, California: Final Technical Report*: U.S. Geological Survey (USGS), Contract Number 14-08-0001-21950, 26p.

Cotton, William and Associates, Inc. and Allan E. Seward Engineering Geology, Inc. 1984. *Engineering Geological Investigation of the San Gabriel Fault*: Report prepared for the Newhall Land and Farming Company, Valencia, California, Volume I and II, 34p.

County of Los Angeles, Drinking Water Standards, Requirements for Well Construction/Decommissioning: Department of Public Health, Environmental Health, Bureau of Environmental Protection, 2p.

Crook, R., Jr., C.R. Allen, B. Kamb, C.M. Payne and R.J. Proctor. 1987. *Quaternary Geology and Seismic Hazard of the Sierra Madre and Associated Faults, Western San Gabriel Mountains*: U.S. Geological Survey (USGS) Professional Paper 1339, pp. 27–63.

Crowell, J.C. 1952. *Probable Large Lateral Displacement on San Gabriel Fault, Southern California*: American Association of Petroleum Geologist Bulletin Volume 36, Number 10, pp. 2026-2035.

Crowell, J.C. 2003. *Tectonics of Ridge Basin Region, Southern California*: Geological Society of America Special Paper 367, pp. 157–203.

Davis, T.A. and J.L. Shelton. 2014. *Groundwater-Quality Data in the Santa Cruz, San Gabriel, and Peninsular Ranges Hard Rock Aquifers Study Unit, 2011–2012—Results from the California GAMA Program*: U.S. Geological Survey Data Series 874, 142p., available at: **http://dx.doi.org/10.3133/ds874**.

Dawson, T.E., and R.J. Weldon. 2013. *Appendix B – Geologic Slip Rate Data and Geologic Deformation Model in Field, et al. 2013. Uniform California earthquake rupture forecast, version 3 (UCERF3)—The time-independent model*: U.S. Geological Survey (USGS) Open-File Report 2013–1165, and California Geological Survey (CGS) Special Report 228.

Deere, D.U. and D.W. Deere. 1989. *Rock Quality Designation (RQD) After Twenty Years*: U.S. Army Corps of Engineers (USACE), Report GL-89-1, 67p.

Deere, D.U. 1964. *Technical Description of Rock Cores for Engineering Purposes*: Rock Mechanics and Engineering Geology, Volume 1, Number 1, pp. 17-22.

Ehlig, P.L. 1975a. Geologic *Framework of the San Gabriel Mountains in San Fernando, California, Earthquake of 9 February 1971*: California Division of Mines and Geology Bulletin 196, pp. 7-18.

______. 1975b. *Basement Rocks of the San Gabriel Mountains, South of the San Andreas Fault, Southern California*: California Division of Mines and Geology Special Report 118, pp. 177-185.

Field, E.H., G.P. Biasi, P. Bird, T.E. Dawson, K.R. Felzer, D.D. Jackson, K.M. Johnson, T.H. Jordan, C. Madden, A.J. Michael, K.R. Milner, M.T. Page, T. Parsons, P.M. Powers, B.E. Shaw, W.R. Thatcher, R.J. Weldon II, and Y. Zeng. 2013. *Uniform California earthquake rupture forecast, version 3 (UCERF3)—The time-independent model*: U.S. Geological Survey (USGS) Open-File Report 2013–1165, and California Geological Survey (CGS) Special Report 228, 97p.

Fell, R., P. MacGregor, D. Stapledon, and G. Bell. 2005. *Geotechnical Engineering of Dams.* Taylor & Francis Group: London, UK.

Franklin, J.A. and R. Chandra. 1972. *The Slake Durability Index*: International Journal of Rock Mechanics and Mining Sciences & Geomechanics Abstracts, Volume 9, Number 3 pp. 325-342.

Freeze, R.A. and J.A. Cherry. 1979. *Groundwater*: Englewood Cliffs, NJ, Prentice-Hall, 604p.

Fugro William Lettis & Associates, Inc. (FWLA). 2010a. Technical Memorandum: Verdugo Fault Crossing of Los Angeles to Palmdale Segment, California High-Speed Train Project. September 15.

______ (FWLA). 2010b. Technical Memorandum: Whitney Fault Crossing of Los Angeles to Palmdale Segment, California High-Speed Train Project. October 12.

______ (FWLA). 2010c. Technical Memorandum: Agua Dulce Fault Zone Crossing of Los Angeles to Palmdale Segment, California High-Speed Train Project. October 15.

Fuis, G.S., Ryberg, T., Godfrey, N.J., Okaya, D.A., and Murphy, J.M. 2001. Crustal structure and tectonics from the Los Angeles basin to the Mojave Desert, southern California: Geology, Volume 29, Number 1, pp. 15-18.

Fuis, G. S, Clayton, R. W. Davis, P. M., Ryberg, T., Lutter, W. J., Okaya, D. A., Hauksson, E., Prodehl, C., Murphy, J. M., Benthien, M. L., Baher, S. A., Kohler, M. D., Thygesen, K., Simila, G., and Keller, G. R. 2003. Fault systems of the 1971 San Fernando and 1994 Northridge earthquakes, southern California: relocated aftershocks and seismic images from LARSE II: Geology, Volume 31, Number 2, pp. 171–174.

Fumal, T.E., A.B Davis, W.T. Frost, J. O'Donnell, G. Sega, and D.P. Schwartz. 1995. Recurrence studies of Tujunga segment of the 1971 San Fernando, California, earthquake: EOS Transactions, American Geophysical Union Supplement, Volume 76, Number 46, pp. 364.

Gamble, J.C. 1971. *Durability-Plasticity Classification of Shales and other Argillaceous Rocks.* Ph.D. thesis, University of Illinois.

Geokon. no date. *LogView, Version 3.0.*

Geokon. 2014. *Instruction Manual Model 4500 series Vibrating Wire Piezometers.*

Goel, R.K., J.L. Jewtha, and A.G. Paithankar. 1996*. Correlation Between Barton's Q and Bieniawski's RMR – A New Approach*: International Journal of Rock Mechanics and Mining Sciences & Geomechanics Abstracts, Volume 33, Number 2, pp. 179-181.

Heaton, T.H. 1982. *The 1971 San Fernando earthquake; a double event*: Bulletin of the Seismological Society of America, Volume 72, Number 6, pp. 2037-2062.

Hendrix, E.D. and R.V. Ingersoll. 1987. *Tectonics and alluvial sedimentation of the upper Oligocene/lower Miocene Vasquez Formation, Soledad basin, southern California*: Geological Society of America Bulletin, Volume 98, Number 6 pp. 647-663.

Hitchcock, C.S., and C.J. Wills. 2000. *Quaternary Geology of the San Fernando Valley, Los Angeles County, California*: California Division of Mines and Geology (CDMG) Map Sheet 50, Scale 1:48,000.

Hoek, E., T.G. Carter, and M.S. Diederichs. 2013. *Quantification of the Geological Strength Index Chart*: 47th United States Rock Mechanics/Geomechanics Symposium. San Francisco, California, USA.

Hoek, E. 2007. *Practical Rock Engineering*: Available at: http://www.rocscience.com/hoek/PracticalRockEngineering.asp

Hoek, E., P.K. Kaiser, and W.F. Bawden. 1995. *Support of Underground Excavations in Hard Rock.* Rotterdam: A.A. Balkema.

International Society for Rock Mechanics (ISRM). 2015. *The ISRM Suggested Methods for Rock Characterization, Testing and Monitoring: 2007-2014.* Published by Springer International Publishing, Switzerland, Editor, E. Ulusay, 293p.

______ (ISRM). 1978. *Suggested Methods for the Quantitative Description of Discontinuities in Rock Masses*: International Journal of Rock Mechanics, Mining Sciences, and Geomechanics, Volume 15, Number 5, pp. 319-368.

Kamerling, M.J. and B.P. Luyendyk. 1985. *Paleomagnetism and Neogene Tectonics of the Northern Channel Islands, California*: Journal of Geophysical Research, Volume 90, Number B14, pp. 12485-12502.

Kew, W.S.W. 1924. *Geology and oil resources of a part of Los Angeles and Ventura Counties, California*: U.S. Geological Survey Bulletin 753, scale 1:62,500, 202p.

Koterba, M.T., F.D. Wilde, and W.W. Lapham. 1995. *Groundwater Data-Collection Protocols and Procedures for the National Water-Quality Assessment Program—Collection and Documentation of Water-Quality Samples and Related Data*: U.S. Geological Survey Open-File Report 95–399, 114p.

Lancaster, J.T., J.L. Hernandez, W.D. Haydon, T.E. Dawson and C.A. Hayhurst. 2012. *Plate 22, Geologic Map of Quaternary Surficial Deposits in Southern California, Lancaster 30'X60' Quadrangle*, scale 1:100,000, *in* Bedrossian, P.D, Roffers, C.A., Hayhurst, J.T., and Short, W.R. (compilers), **Geologic Compilation of Quaternary Surficial Deposits in Southern California**: California Geological Survey Special Report 217, 21p.

Leighton, K.A. and S.P. Philips. 2003. *Simulation of Ground-water Flow and Land Subsidence in the Antelope Valley Groundwater Basin, California*: U.S. Geological Survey Water-Resources Investigation Report 03-4016, 118p.

Lindvall, S.C. and C.M. Rubin. 2003. *Slip Rate Studies along the Sierra Madre-Cucamonga Fault System Using Geomorphic and Cosmogenic Surface Exposure Age Constraints*: U.S. Geological Survey (USGS), NEHRP External Grant Award Number 03HQGR0084, 13p.

Los Angeles County Department of Public Works (LADPW). 2006. *Hydrology Manual*. Water Resources Division: Alhambra, California. Available at: http://dpw.lacounty.gov/wrd/publication/.

______ (LADPW). 2014. *Greater Los Angeles County Region Integrated Resource Water Management Plan*. Available at: http://www.ladpw.org/wmd/irwmp/.

Marinos, P., and E. Hoek. 2000. *GSI-A geologically friendly tool for rock mass strength estimation*: Proceedings to GeoEng 2000 Conference. Melbourne, pp. 1422-1442.

McCulloh, T.H., L.A. Beyer, R.W. Morin. 2001. *Mountain Meadows Dacite: Oligocene Intrusive Complex that Welds Together the Los Angeles Basin, Northwestern Peninsular Ranges, and Central Transverse Ranges, California*: U.S. Geological Survey (USGS) Professional Paper 1749, 34p.

Murphy, L.M. (Editor). 1973. *San Fernando, California, Earthquake of February 9, 1971, Volume III, Geological and Geophysical Studies*: National Oceanic and Atmospheric Administration (NOAA). 432p.

National Climate Data Center (NCDC). 2007. Access at http://www.ncdc.noaa.gov/oa/ncdc.html.

National Park Service (NPS). 2013. San Gabriel Watershed and Mountains Special Resource Study and Environmental Assessment, 316p. Available at: http://www.nps.gov/pwro/sangabriel.

Nourse, J.A. 2002 *Middle Miocene Reconstruction of the Central and Eastern San Gabriel Mountains, Southern California, with Implications for Evolution of the San Gabriel Fault and Los Angeles Basin*: Geological Society of America Special Paper 365, pp. 161-185.

Oakeshott, G.B. 1946. *Titaniferous Iron-ore Deposits of the Western San Gabriel Mountains, Los Angeles County, California*: California Division of Mines and Geology Bulletin 129 pp. 245-266.

______. 1958. *Geology and Mineral Deposits of San Fernando Quadrangle, Los Angeles County, California*: California Division of Mines and Geology Bulletin 172, 147p.

Olson, B.P.E. and J.L. Hernandez. 2013. Preliminary Geologic Map of the Palmdale 7.5' Quadrangle, Los Angeles County, California: A Digital Database, version 1.0: California Geological Survey, scale: 1:24,000.

Parsons Brinkerhoff. 2011. Notice to Designers No. 1 – Geotechnical Investigations for Preliminary Design.

______. Notice to Designers No. 8 – Geotechnical Boring and Sample Identification, Handling and Storage Guidelines.

Piper, A.M. 1944. *A Graphic Procedure in the Geochemical Interpretation of Water Analyses*: Eos Transactions, American Geophysical Union, Volume 25, Number 6, pp. 914-923.

Powell, R.E. 1993. *Balanced Palinspastic Reconstruction of Pre-late Cenozoic Paleogeology, Southern California; Geologic and Kinematic Constraints on Evolution of the San Andreas Fault System*: Geological Society of America Memoir 178, pp. 1-106.

Rocscience. 2016. *Dips, Version 7.004.*

Rostami, J. and L. Ozdemir. 1993. *A new model for performance prediction of hard rock TBMs.* RETC conference proceedings, June 13-17, Boston, MA.

Rostami, J. 1991. *Design optimization, performance prediction, and the economic analysis of TBM application for the construction of proposed Yucca Mountain nuclear waste repository.* Thesis No. 3941, Colorado School of Mines, Golden, CO.

Rupert, M.G. and L.N. Plummer. 2004. *Ground-Water Flow Direction, Water Quality, Recharge Sources, and Age, Great Sand Dunes National Monument, South-Central Colorado*, 2000–2001: U.S. Geological Survey (USGS) Scientific Investigations Report 2004–5027, 28p.

Saul, R.B. and T.M. Wootton. 1983*. Geology of the south half of the Mint Canyon quadrangle, Los Angeles County, California*: California Division of Mines and Geology (CDMG) Open File Report 83-24 LA, 139 p., maps, scale 1:9,600.

Seed, H.B., R.J. Woodward, and R. Lundgren. 1962. *Prediction of Swelling Potential for Compacted Clays*: Journal of Soil Mechanics and Foundations Division, ASCE, Volume 88, Number 3 pp. 53-87.Siade, A.J., T. Nishikawa, D.L. Rewis, P. Martin, and S.P. Phillips. 2014. *Groundwater-flow and land-subsidence model of Antelope Valley, California*: U.S. Geological Survey Scientific Investigations Report 2014–5166, 136p.

Siade, A.J., T. Nishikawa, D.L. Rewis, P. Martin, and S.P. Phillips. 2014. Groundwater-flow and land-subsidence model of Antelope Valley, California: U.S. Geological Survey Scientific Investigations Report 2014–5166, 136p.

Sieh, K.E. 1978. *Slip along the San Andreas fault associated with the great 1857 earthquake*: Bulletin of the Seismological Society of America, Volume 68, Number 6, pp.1421-1448.

Silver, L.T. 1971. *Problems of crystalline rocks of the Transverse Ranges*: Geological Society of America Abstracts with Programs, Volume 3, Number 2, pp. 193-194.

Skempton, A.W. 1953. *The Collodial Activity of Clays*: Proceedings, Third International Conference on Soil Mechanics and Foundation Engineering, Volume I, pp. 57-61.

Stiff, H.A., 1951. *The Interpretation of Chemical Water Analysis by Means of Patterns*: Journal of Petroleum Technology, Volume 3, Number 10, pp. 15-17.

Sullwold Jr., H.H. 1960. *Tarzana Fan, deep submarine fan of Late Miocene age, Los Angeles County, California*: American Association of Petroleum Geologists Bulletin, Volume 44, Number 4, pp. 433-457.

Taylor, C.B. and W. Reother. 1982. *A Uniform Scale for Reporting Low-Level Tritium Measurements in Water*: International Journal of Applied Radioactive Isotopes, Volume 33, Number 5, pp. 377–382.

U.S. Department of the Interior Bureau of Reclamation. 1998. *Engineering Geology Field Manual. Volumes 1 and 2*: Available at: http://www.usbr.gov/pmts/geology/geoman.html.

U.S. Forest Service (USFS). 2005*. Forest Land and Resources Management Plan, Angeles National Forest, Arcadia, California*: Available: http://www.fs.fed.us/r5/angeles.

U.S. Geological Survey (USGS) Staff. 1971. *Surface faulting, in The San Fernando, California, Earthquake of February 9, 1971*: U.S. Geological Survey Professional Paper 733, p. 55-76.

______ (USGS). 2004*. Geologic Setting of the Transverse Ranges Province – San Gabriel Mountains*: USGS Southern California Aerial Mapping Project (SCAMP). Website last updated September 3, 2004.

______ (USGS). 2016. National Hydrography Dataset (NHD), USGS website, available at: http://nhd.usgs.gov/.

______ (USGS). 1995. Acton Quadrangle, Los Angeles County, California 7.5-Minute Series Topographic Map, scale 1:24,000.

______ (USGS). 1995. Agua Dulce Quadrangle, Los Angeles County, California 7.5-Minute Series Topographic Map, scale 1:24,000.

______ (USGS). 1995. Condor Peak Quadrangle, Los Angeles County, California 7.5-Minute Series Topographic Map, scale 1:24,000.

______ (USGS). 1995. Mint Canyon Quadrangle, Los Angeles County, California 7.5-Minute Series Topographic Map, scale 1:24,000.

______ (USGS). 1995. San Fernando Quadrangle, Los Angeles County, California 7.5-Minute Series Topographic Map, scale 1:24,000.

______ (USGS). 1995. Sunland Quadrangle, Los Angeles County, California 7.5-Minute Series Topographic Map, scale 1:24,000.

U.S. Geological Survey (USGS) and California Geological Survey (CGS). 2006. Quaternary Fault and Fold Database for the United States. Accessed September 28, 2016 from USGS website: http//earthquakes.usgs.gov/hazards/qfaults/.

U.S. Department of Transportation Federal Highway Administration (FHWA). 2009. Technical Manual for Design and Construction of Road Tunnels – Civil Elements. Washington D.C., March 2009.

______ (FHWA). 2002. *Geotechnical Engineering Circular No. 5 Evaluation of Soil and Rock Properties*: Washington D.C.

Wallace, R.E. 1990. *The San Andreas Fault System, California*: U.S. Geological Survey (USGS) Professional Paper 1515, 283p.

Waterloo Hydrogeologic. 2016. *AquiferTest Pro, version 2016.1.*

Weber, F.H., J.H. Bennett, R.H. Chapman, G.W. Chase, R.B. and Saul. 1980. *Earthquake hazards associated with the Verdugo-Eagle Rock and Benedict Canyon fault zones, Los Angeles County, California*: California Division of Mines Geology (CDMG) Open-File Report 80-10 LA.

Weber, F.H., Jr.,1982. *Geology and Geomorphology along the San Gabriel Fault Zone, Los Angeles and Ventura Counties, California*: California Division of Mines and Geology Open-File Report 82-2 LA, 157p.

Weigand, P.W., A.P. Barth, and P.L. Ehlig. 1989. *Field Trip Guide to a Portion of the Western San Gabriel Mountains, Los Angeles County, California*, *in* Collins, L.G. (editor), Geologic Excursions in the Greater Los Angeles Area: National Association of Geology Teachers, pp. 38-44.

Woodburne, M.O. 1975. *Cenozoic Stratigraphy of Transverse Ranges and Adjacent Areas, southern California*: Geological Society of America Special Paper 162, 91p.

Wyllie, D.C. 1999. *Foundations on Rock, 2nd Edition.* Taylor and Francis, London, UK, 401 pp.

Yerkes, R.F. and W.H.K. Lee. 1987. *Late Quaternary Deformation in the Western Transverse Ranges, California*: U.S. Geological Survey (USSG) Professional Paper 1339, pp. 71-82.

Yerkes, R.F. and R.H. Campbell. 2005. *Preliminary Geologic Map of the Los Angeles 30'x60' Quadrangle, Southern California*: U.S. Geological Survey Open File Report 2005-1019, 2 Sheets, Scale 1:100,000.

APPENDICES

Appendix A – Maps and Profiles

Appendix B – Report Figures

Appendix C – Drilling Summaries

Appendix D – Rock Core Borings

Appendix E – Petrography

Appendix F – Instrumentation

Appendix G – Geophysical Surveys

Appendix H – In-Situ Testing

Appendix I – Soil and Rock Laboratory Testing

Appendix J – Groundwater Laboratory Testing

Appendix K – Rock Mass Characterization